SKB

TECHNICAL REPORT 87-10

Outline of models of water and gas flow through smectite clay buffers

Roland Pusch, Harald Hökmark,
Lennart Börgesson
Swedish Geological Co, Lund

June 1987

SVENSK KÄRNBRÄNSLEHANTERING AB
SWEDISH NUCLEAR FUEL AND WASTE MANAGEMENT CO

BOX 5864 S-102 48 STOCKHOLM
TEL 08-665 28 00 TELEX 13108-SKB

OUTLINE OF MODELS OF WATER AND GAS FLOW THROUGH SMECTITE CLAY BUFFERS

Roland Pusch, Harald Hökmark, Lennart Börgesson

Swedish Geological Co, Lund

June 1987

SWEDISH GEOLOGICAL CO
Roland Pusch/JS

Date: 1987-06-03
ID-no: IRAP 87500

OUTLINE OF MODELS OF WATER AND GAS FLOW THROUGH SMECTITE CLAY BUFFERS

Roland Pusch
Harald Hökmark
Lennart Börgesson

Swedish Geological Co
Lund, Sweden

Key words: Clay, gas conductivity, hydraulic conductivity, hydrous mica, microstructure smectite

CONTENTS

SUMMARY

While routine laboratory tests yield average values of the hydraulic and gas conductivities, the actual rate and capacity of flow is not revealed. Microstructure analyses of natural clays with hydrous mica or smectite as major clay mineral have demonstrated that there are large variations in pore size, and that a few wide pores may be responsible for the great majority of the permeation. A similar behavior may be valid also for "artificially" produced smectite clays which are formed from powdered Na bentonite. A model is derived for such clays in which the powder grains are regarded as anisotropic aggregates which swell on wetting and form a network with pores that are successively filled with a clay gel that emanates from the aggregates. The density and hydraulic conductivity of the gel is a function of the pore size and distribution as well as of the porewater chemistry.

Applying the model to three "reference" clay types of different bulk density, it is shown that realistic data for the hydraulic and gas conductivities as well as for the ratio of the anion and cation diffusion capacities are arrived at. The model is therefore taken as a basis for further development.

1 SCOPE

The conductivity of water and gas have been measured and expressed in terms of average apparent permeabilities in several experiments in the current SKB research on buffer materials. While such flow data are valuable for characterizing and comparing the perviousness of soil-type materials, they do not reveal the actual flow rate in the pore system or the degree of uniformity of the flow across a permeated section. Since the flow rate is a determinant of internal erosion and therefore of the physical stability of the microstructure, and the actual flow distribution determines the extent and rate to which mineral alteration and attack on embedded metal canisters take place, the flow pattern needs to be characterized in greater detail in order to allow for the prediction of physical and chemical effects of the types mentioned. As to gas permeation, earlier investigations have revealed the major mode of penetration but it needs to be further examined and related to the actual geometrical features of the pore system.

In this report a number of experimental results are compiled and correlated with microstructural data to form a basis for the formulation of physical models for water and gas flow through montmorillonitic buffer materials. Preliminary mathematical analogies are also outlined.

The report is confined to montmorillonite clay with a density varying from that of highly compacted Na bentonite to the soft state of smectite gel pore fillings in clay/ballast mixtures.

2 CLAY MICROSTRUCTURE

2.1 General influence on water and gas flow rates

2.1.1 Water

As for other porous media, the hydraulic conductivity of montmorillonitic clays is influenced by mechanical effects, particularly the void size distribution and tortuosity of the flow passages (1). It is a wellknown fact that the average hydraulic conductivity k is more than two orders of magnitude lower than that of hydrous mica ("illite") which in turn is more than two orders of magnitude lower than that of kaolinite (Fig 1). The reason for these differences is that the coefficient of permeability is largely controlled by the tendency of the clay to disperse and form aggregates, the most surface-active mineral montmorillonite forming the most homogeneous, low-pervious particle system. Relationships of the sort shown in the diagram have been found to be in agreement with semi-empirical expressions of the average hydraulic conductivity of soils, like Taylor's simple flow equation (Eq. 1) and Kozeny-Carman's expression (Eq. 2). The first-mentioned relationship is based on Poiseuille's law, considering the soil to behave as a bundle of capillary tubes, while the other is an expression for the permeability of porous media.

$$k = D_s^2 \frac{\rho_w}{\eta} \cdot \frac{e^3}{(1+e)} C \qquad (1)$$

where k = Darcy coefficient of permeability
D_s = "effective" particle diameter
ρ_w = unit weight of water
η = viscosity of water
e = void ratio

$$k = \frac{\rho_w}{k_o S^2 \eta} \cdot \frac{e^3}{(1+e)} \qquad (2)$$

where k_o = factor depending on pore shape (tortuosity) and ratio of length of actual flow path to soil bed thickness
S = specific surface area

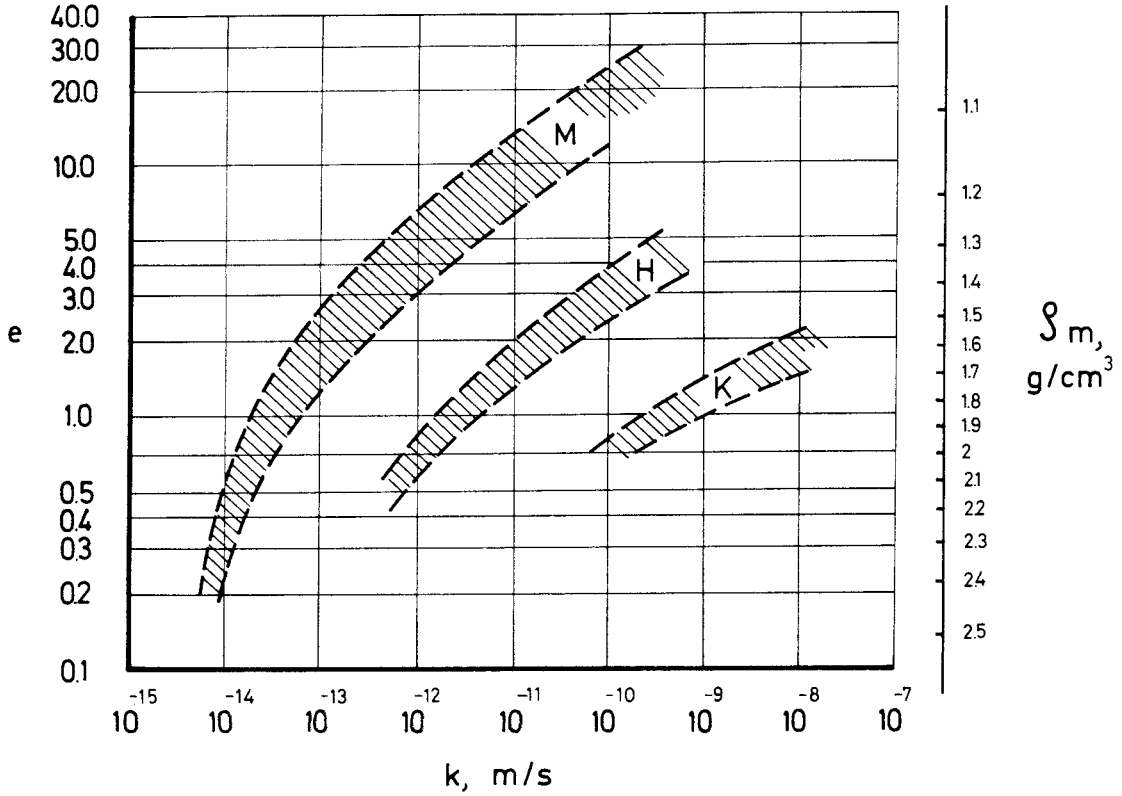

Fig 1. Generalized diagram of the Darcy coefficient of permeability (k) of "pure" clays versus void ratio (e) and bulk density (ρ_m) at complete water saturation. M represents montmorillonite, H hydrous mica, and K kaolinite

We see that the microstructure is a determinant of the flow rate in both expressions, i.e. in terms of "capillary diameter" in Eq. 1, and in the form of pore shape and specific surface area in Eq. 2. The latter equation can be put in the form of Eq. 3, in which A can be taken as a constant for any particular mineral composition, temperature, and microstructural condition (2). The latter may be quite

different in artificially mixed and compacted soils, and it may vary very much also in natural sediments depending on the chemistry of the water and on the rate of sedimentation at their formation.

$$k = A \frac{(\rho_s - \rho_d)^3}{\rho_d^2} \qquad (3)$$

where ρ_s = unit weight of minerals
ρ_d = dry density

A most important mechanical, or rather microstructural, effect is implicitely given by Fig 1 and that is the insignificant drop in permeability when the void ratio is decreased below 0.5. It means that the flow equations do not apply well at a void ratio lower than this figure and that there are permeable passages that persist even at extremely high compression pressures. This fact is of great practical concern and will be focussed on in the report.

2.1.2 Gas

Although gas permeation of water saturated smectite clay has not been investigated to the same extent as water percolation, it is clear that it is transported in a totally different manner. Actually, the microstructure appears to be even more important than it is for water flow in the sense that gas penetrates soil-type materials along a small number of passages when a certain critical gas pressure has been reached. Such channels are assumed to be formed along intrinsic weak parts of the microstructure. At lower pressures migration takes place in the form of diffusion of dissolved gas.

2.2 Interaction and arrangement of montmorillonite crystallites

2.2.1 General

While early concepts of clay structure generally implied single plate interaction, the model of multiple-plate assemblages (3) has recently been validated for all sorts of aged clays (4, 5). According to this model the individual clay particles form aggregates separated by

voids of different size and interconnectivity. This is shown by Fig 2, which also illustrates the influence of porewater chemistry on the microstructure.

A number of interparticle bond types are operative in the aggregates of consolidated clays. It can be assumed that a significant fraction of adjacent particles has edge-to-face, direct mineral contacts with primary valence bonds, and van der Waals bonds as major attraction forces, while hydrogen and covalent bonds are minor contributors to the attraction. Electrical double-layers are developed on free basal planes tending to separate the particles. As to montmorillonite in lithium and sodium form, the "particles" consist of stacks of coherent flakes or lamellae separated by water which can be understood as rather rigid water molecule lattices.

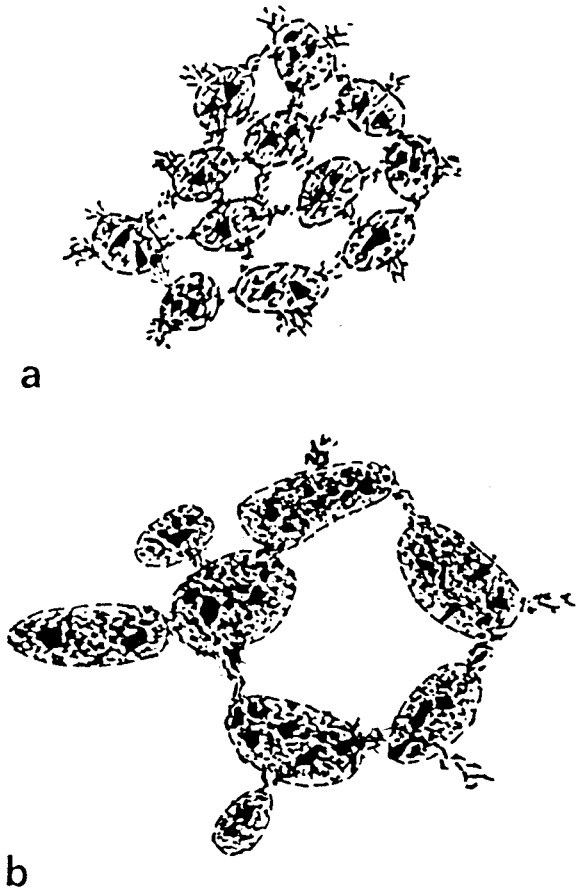

Fig 2. Schematic clay particle arrangement. a) Clay deposited in fresh water with relatively porous aggregates and small voids. b) Marine clay with large, dense aggregates separated by large voids

2.2.2 Na montmorillonite

As in clays with hydrous mica, chlorite and kaolinite as major clay minerals, the multiple-plate microstructure holds also for Na montmorillonite (6). Thus, Na montmorillonite clay consists of stacks, which are thick and comprise several flakes at high bulk densities and which persist after expansion but with a smaller number of flakes (Fig 3). It is concluded from ongoing studies that the continuity of the particle network is preserved even at large expansion, and this has a great impact on the erodibility of soft gels such as those used for rock grouting.

The interaction between montmorillonite flakes and interlamellar water is concluded to give this ordered, "internal" water an energy state that is similar that of ice (7). Probably, only 2 or 3 hydrates are hosted in each interlamellar space and they remain immobile between the flakes even at high hydraulic gradients. Thus, only "external" water in continuous voids is expected to flow under the influence of differential piezometric heads. The location of this mobile water, which is a major issue in the present context, is determined by the microstructure. The matter will be treated in detail in the subsequent text.

For the sake of simplicity we will still use the term particle for individual microstructural constituents in the subsequent text together with the specifications "flake" and "lamella" for individual crystal sheets, "stacks" for aligned, regularly ordered sheets, and "aggregate" for coherent groups of non-oriented sheets and stacks.

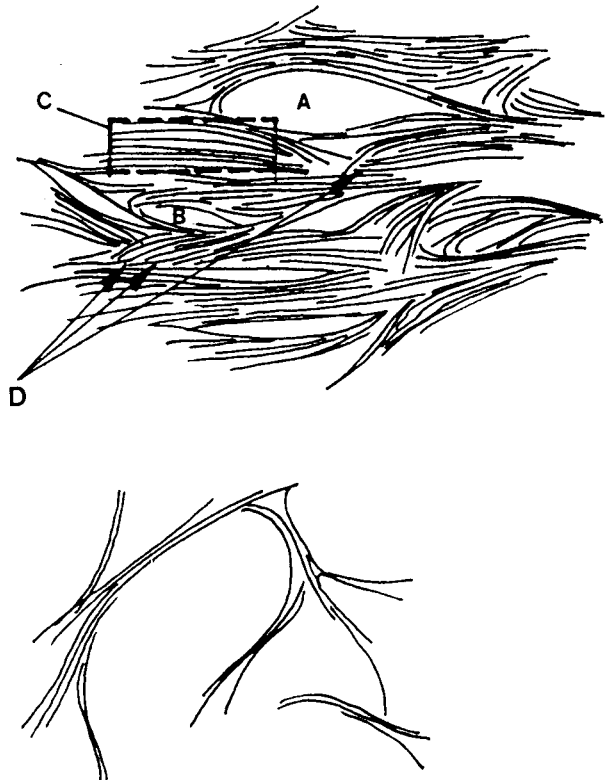

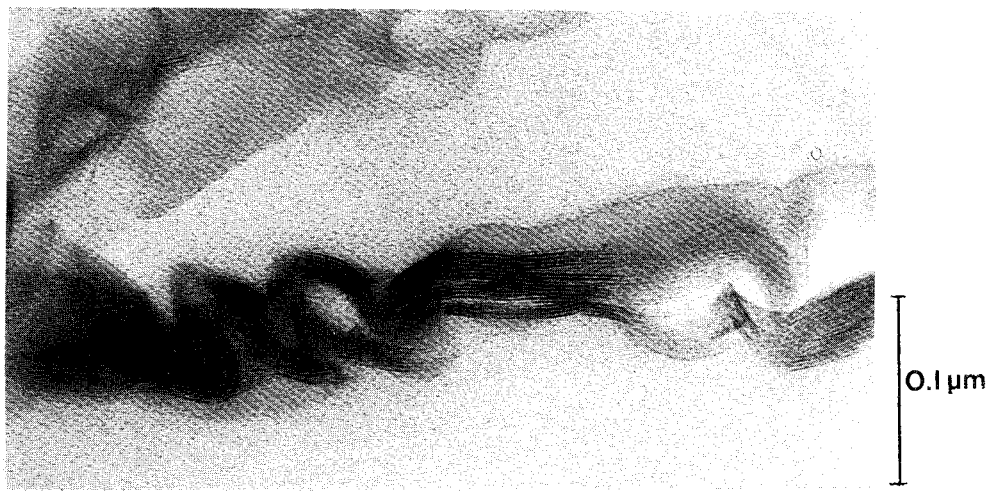

Fig 3. Upper: Dense Na montmorillonite clay. A) Large pore, B) Small void with external water, C) Stack or "quasicrystal" with organized interlamellar water, D) Interface between stacks. Middle: Expanded Na montmorillonite gel with very thin stacks and practically only external water. Lower:TEM picture of expanded Na montmorillonite (Photo: O. Touret)

2.3 Quantitative microstructural analysis

2.3.1 Experimental technique, definitions

The evaluation of microstructural features that are relevant to the hydraulic conductivity is suitably made by applying transmission electron microscopy and ultra-microtomy (3). Micrographs obtained from ultra-thin sections represent two-dimensional, vertical sections through the clay matrix and this offers a possibility of applying simple statistical methods to describe the structural patterns. The total pore area (P) in percent of the total area (T) of micrographs, and the pore size (a_p), are suitable microstructural parameters for the present purpose, the pore size being defined as the longest intercept. The measurement of pore size (individual measurement) and pore area (continuous line integration) are suitably based on drawn images of the micrographs in which no discrete particles are depicted. Hence, the drawings show black areas for the clay particle matrix with no sectioned pore space (Fig 4). Depending on particle size and arrangement this matrix has a varying density which is not illustrated by the depicted, uniformly black areas and this means that the true porosity cannot be evaluated from the drawings. The sections contain very small pores which are embedded in the clay sections and which are thus not revealed, but because they do not represent flow paths it is acceptable to omit them. An example of the relevance of the P/T parameter is given in Fig 5, which illustrates the coagulation effect of salt water on clay microstructure. Thus, P/T is much higher for soft marine and brackish-water clays than for fresh-water clays with similar preconsolidation pressures and water contents. We will see later that this parameter is also related to the hydraulic conductivity and that a_p is a particularly important measure of how microstructural features control water percolation of clays.

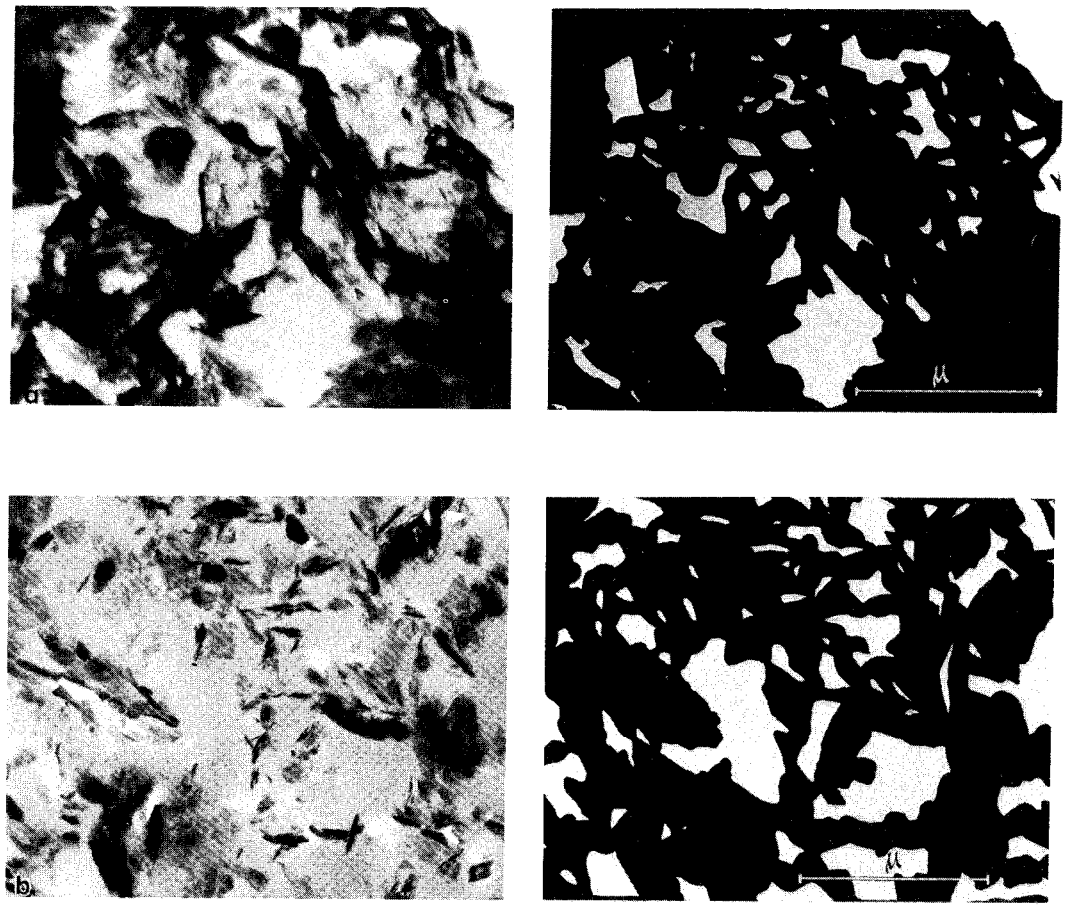

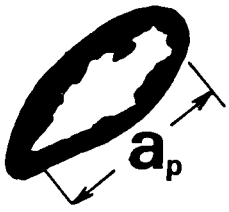

Fig 4. Example of schematic reproduction of electron micrographs. The continuous particle network is marked black without reference to variations in density. The pore system consisting of discrete, sectioned pores defined in the picture, is marked white

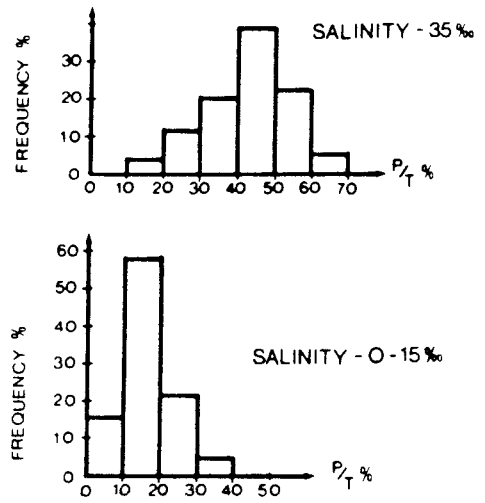

Fig 5. P/T versus salinity of Quaternary clays with hydrous mica as major clay mineral (8)

2.3.2 Microstructure of natural clays

The microstructure of illitic clays has been investigated in great detail and a large number of characteristic microstructural data have been gained (3). Characteristic pore size data of clays with bulk densities ranging between 1.3 and 1.6 t/m^3 are shown in Table 1, in which the distribution of the pore size is expressed in terms of the median and quartile values as well as of the 95-percentile. The latter reflects the content of "micro-pores" and "fine" pores according to Oden's classification (Table 2) which are the major contributors to the P/T value. The data, which are assumed to be representative of smectite-poor clays of quite different mineral compositions, are confined to those which can be evaluated from electron micrographs covering cross sections of 50-100 μm^2. A more complete picture of the pore size distribution would require that very large cross section areas are analyzed and this has been made in more recent studies.

Table 1 The structural parameter P/T and median values, quartiles and percentile P_{95} of the pore size a_p (Hydro-mica clays)

Site	Depth m	P/T %	a_p in µm M	Q_1	Q_3	P_{95}
Skå-Edeby	2.0	17.4	0.21	0.14	0.34	0.70
	5.0	9.4	0.11	0.08	0.20	0.50
	7.0	13.8	0.13	0.10	0.19	0.35
	8.0	21.5	0.24	0.18	0.40	0.80
	9.0	24.9	0.20	0.14	0.31	0.70
	10.0	11.3	0.19	0.11	0.32	0.70
Lilla Edet	3.0	37.5	0.15	0.06	0.25	1.10
	3.0	48.4	0.14	0.09	0.25	1.30
	6.0	49.3	0.13	0.09	0.25	0.95
	19.0	39.7	0.14	0.10	0.28	1.00
Morjärv	4.0	57.0	0.21	0.14	0.43	1.50
	6.0	45.2	0.33	0.22	0.55	2.50
	9.0	56.2	0.35	0.25	0.60	2.00

M = Median value

Q_1 = Lower quartile

Q_3 = Upper quartile

Table 2 Oden's size classification

>200	µm	Coarse
200-20	"	Medium
20- 2	"	Fine
2- 0.2	"	Micro-
<0.2	"	Ultra-

Similar analyses have been made of dense pre-Quaternary clays of which characteristic data are given in Table 3. These clays, some of

which contain smectite and are therefore of particular interest, have a bulk density ranging between about 1.9 and 2.2 t/m^3. The table illustrates the interesting fact that the pore size distribution of the dense clays is very similar to that of the soft clays. Yet, there is a great difference in the frequency of large voids and the reason for this is that such voids, which are numerous in soft sediments, are primarily compressed in the course of consolidation, leaving the "ultra-pores" unaffected (Fig 6). This is manifested by a difference in P/T, which is in the range of 1.5-15.8 % for the dense clays (with exception of the Silurian clay) and between 11.3 and 57 % for the soft clays with the exception of the extremely fine-grained Ancylus clay from 5 m depth. Obviously, this difference is due to a higher frequency of voids with a diameter exceeding about 0.5-0.8 μm in the soft clay.

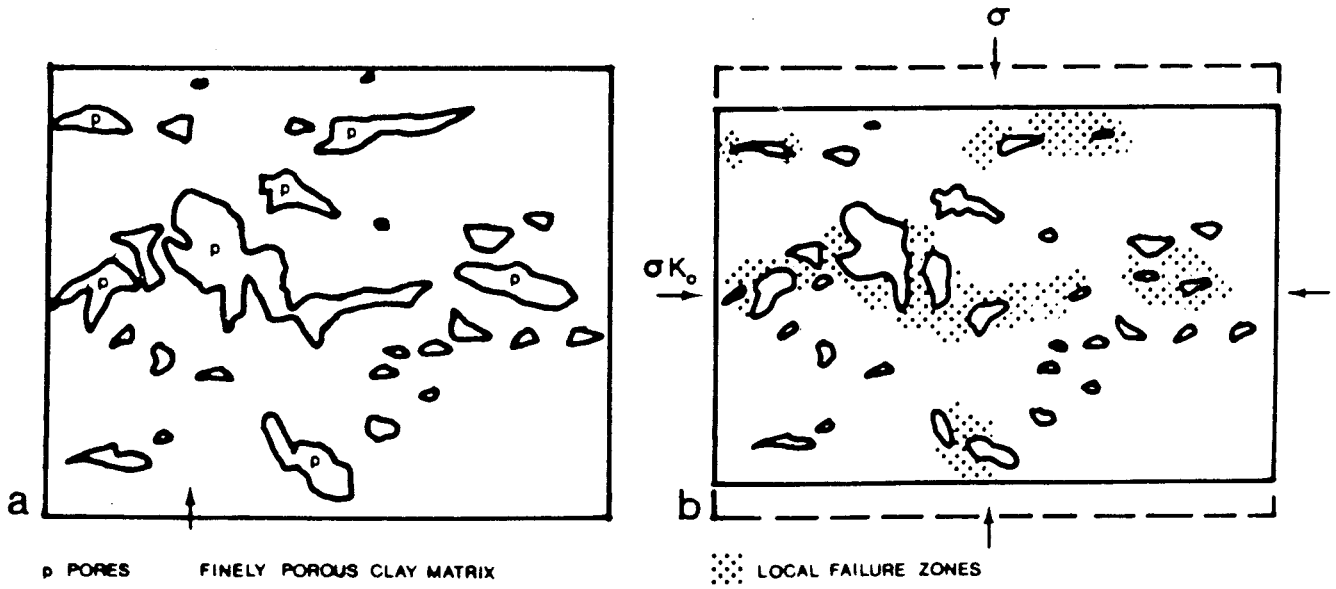

Fig 6. Microstructural changes induced by compression (9). The large voids are primarily compressed while the smaller ones persist

Table 3 Structural parameters of pre-Quaternary, dense clays. The major minerals are given in the right column

Clay sediment	M	a_p in µm Q_1	Q_3	P/T	Clay minerals*	Bulk dens ρ_m, t/m³
Cambrian clay	0.18	0.12	0.30	6.7	H>Chl>K	2.2
Ordovician bent clay	0.12	0.08	0.20	1.5	S>Chl>K	2.0
Silurian clay	0.20	0.14	0.33	37.2	H>Chl	2.2
Triassic clay	0.12	0.09	0.25	7.0	S>H>K>Chl	2.3
Cretaceous kaolin clay	0.11	0.10	0.28	9.3	K	2.1
Cretaceous Fish clay	0.30	0.25	0.45	12.7	S>K	1.9
Tertiary London clay	0.29	0.22	0.50	14.5	H>S>K>Chl	1.9
Tertiary Rosnaes clay	0.33	0.20	0.86	15.8	S>H>K>Chl	1.8

* S = smectite and mixed layer minerals, H = hydrous mica, Chl = chlorite, K = kaolinite

As concerns the influence of different clay minerals we see that the dense, smectite-rich materials, i.e. the Ordovician and Triassic clays, have a smaller variation (Q_3-Q_1) in pore size than the other dense clays (Cambrian, Silurian and Cretacious) and this is attributed to the ability of the smectite component to swell and become homogeneous. This property was obviously not as strong in the two softer smectitic clays.

2.3.3 Microstructure of "artificial" smectite clays

In practically all the comprehensive laboratory tests which have been made of pure bentonites in Sweden, air-dry bentonite powder has been applied in oedometers and confined between fixed filters during water uptake to reach saturation. Since many of the practical repository sealing operations imply that Na bentonite powder is used, it is pertinent to consider the microstructure of such "artificially" produced clays. The individual grains consist of large numbers of more or less aligned stacks of montmorillonite flakes but since the grains are randomly oriented in the powder mass the orientation of flakes is approximately at random also in the saturated state. The homogenization, or maturation process, which is schematically illustrated in

Fig 7, is expected to yield a microstructural pattern that is much more isotropic than in natural smectitic clays, where there is generally a marked alignment of the particles. At high bulk densities the microstructural homogeneity of the compacted material is expected to be very good with a narrow void size spectrum, while a low bulk density would logically imply a larger variation. It is also reasonable to believe that the voids between the powder grains do not become effectively occupied by clay emerging from the expanding grains and that they remain to be primary passage-ways for water and gas even at high bulk densities.

2.3.3.1 Soft Na montmorillonite clay gels

In this context it is of fundamental importance to distinguish between interlamellar space holding "internal" water, and voids which host "external" water (7). The first-mentioned space contains immobile, interlamellar water that forms a large fraction of the total pore volume in smectite-rich clays of high density, while it only represents a minor part at densities lower than about 1.3-1.4 t/m^3 (Fig 8). Naturally, a much larger number of voids combine to form passage-ways for water or gas in soft than in very dense smectite clays. The microstructural evolution that leads to these different conditions can be demonstrated by considering the size distribution of the powder grains (Fig 9) and their arrangement, which is illustrated by the ten random structures shown in Fig 10. The latter is representative of uncompacted backfillings of bentonite powder like that of the SFR slot backfilling, and we will examine one arbitrarily chosen example, i.e. no 1 in Fig 10, to see what the characteristic spread in microstructural density will be on wetting and internal swelling. In order to make our point clear we will consider several cases of grain orientation, the purpose being to illustrate how anisotropic grain swelling yields various degrees of heterogeneity of the microstructural pattern. Fig 11 shows the assumed variation in orientation, while Fig 12 demonstrates the associated variation in bulk density after complete wetting and expansion in one plane, provided that the outer boundaries of the elements remain essentially stationary.

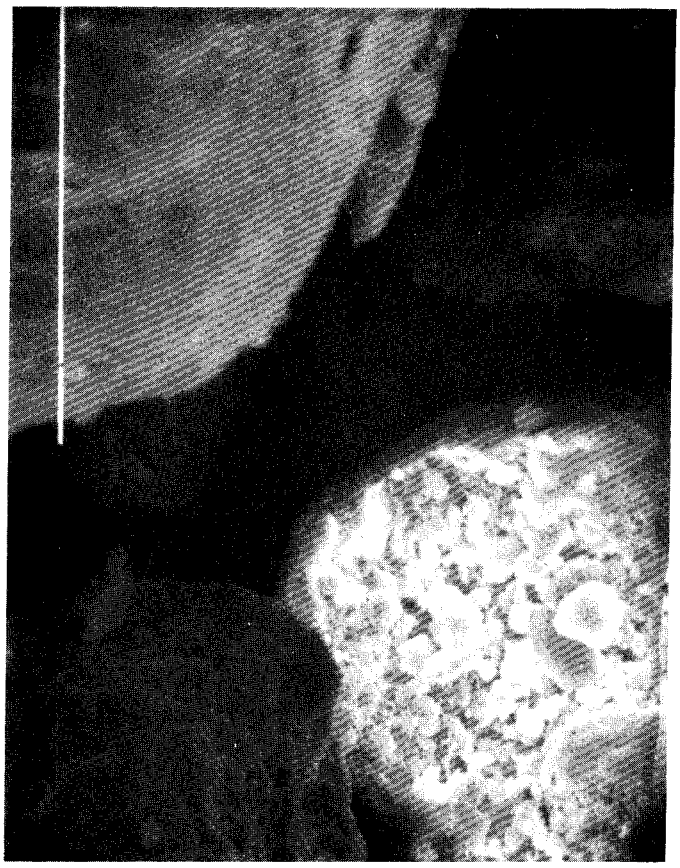

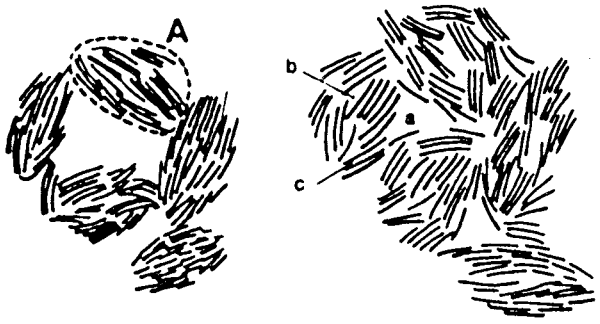

Fig 7. Homogenization of artificially produced Na bentonite clay. Upper: SEM picture of MX-80 powder grains (white line is 10 µm long, photo D.M. Anderson). Lower: Schematic particle arrangement in highly compacted Na bentonite. Left picture: powder grains in air-dry state. Right picture: "homogeneous" state after saturation and particle redistribution. A=grain consisting of stacks of flakes, a and b=voids of various size, c=interlamellar space in stack

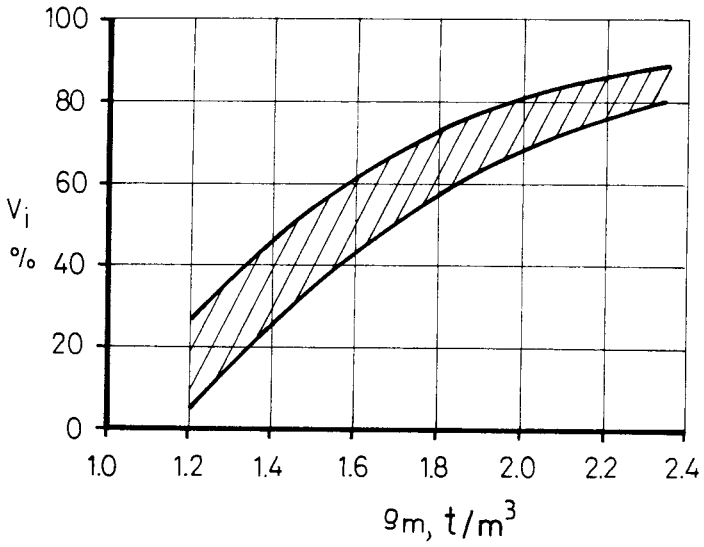

Fig 8. General relationship between bulk density and content of internal water in percent of the total porewater volume of smectite clays

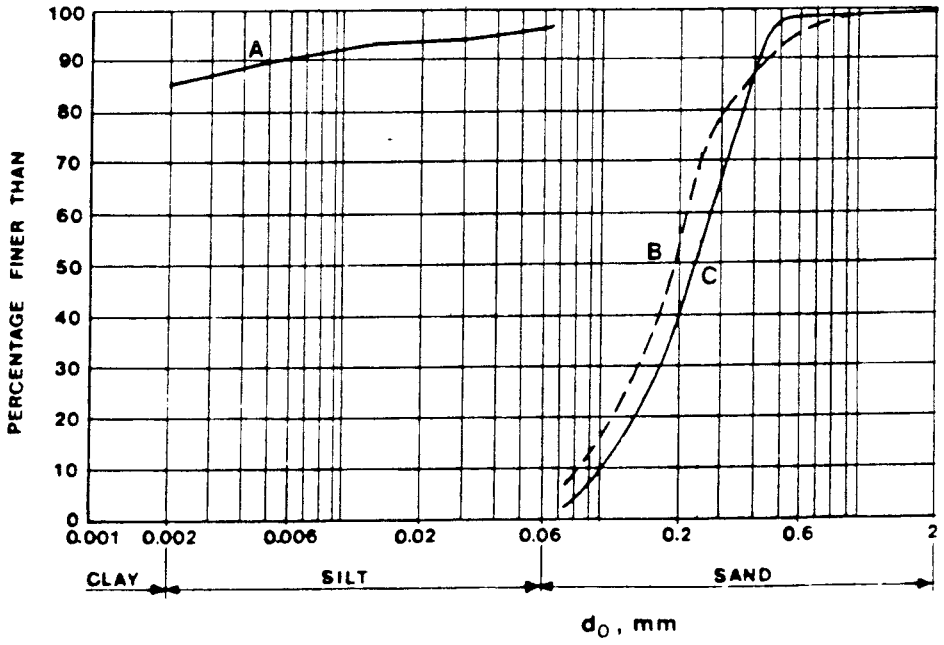

Fig 9. Grain size characteristics of MX-80 Na bentonite powder. A represents the particle size distribution according to sedimentation analyses. B) and C) represent powder from different bulk loads after sieving in air-dry condition

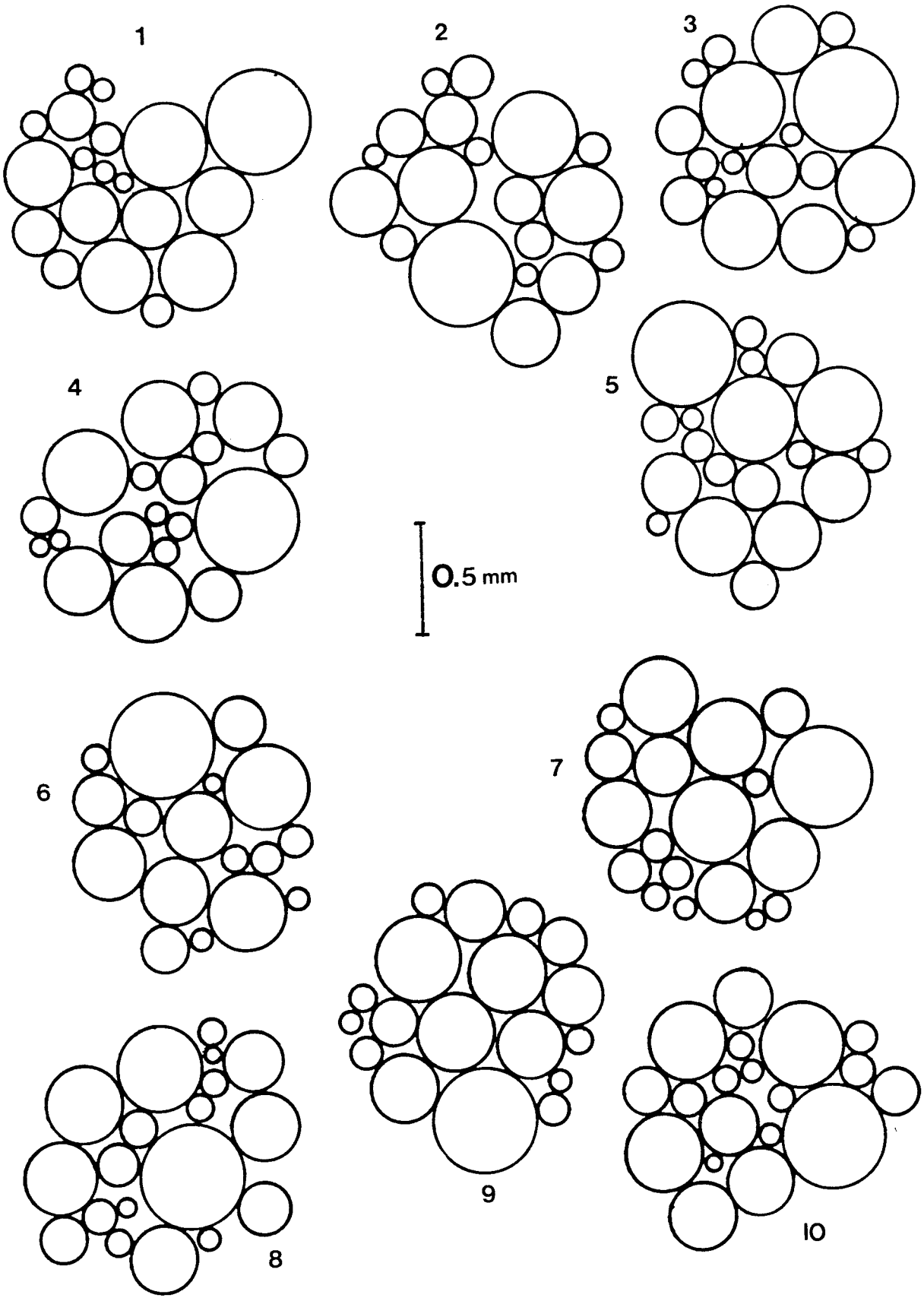

Fig 10. Ten random structures of MX-80 grains

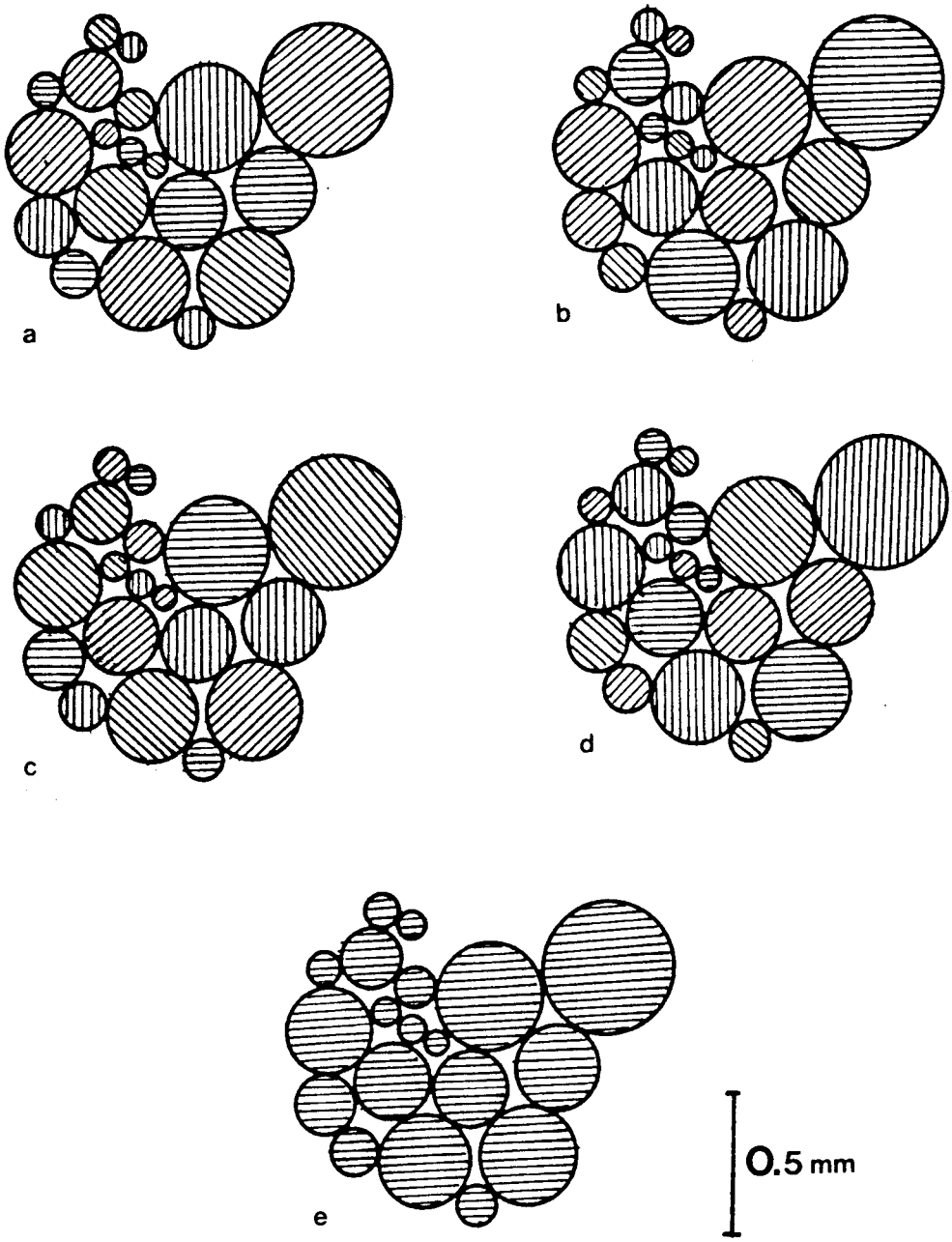

Fig 11. Assumed variation in orientation of MX-80 grains arranged according to no 1 in Fig 10. All crystal ab-planes are taken to be perpendicular to the plane of the paper

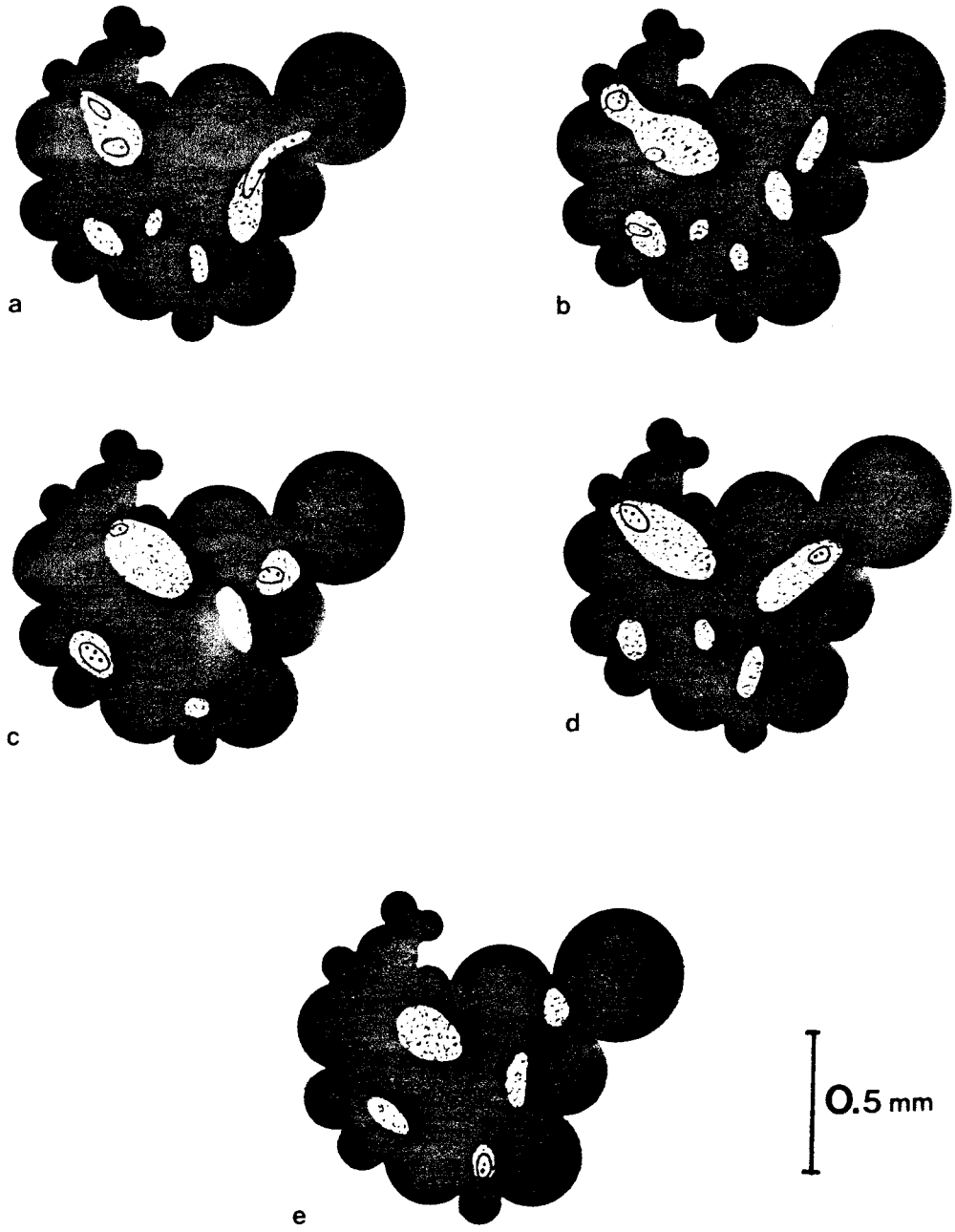

ρ_m = 1.5-1.7 g/cm^3 ρ_m = 1-1.3 g/cm^3 ρ_m = <1.1 g/cm^3

V_i = 30-50 % V_i = 5-25 % V_i = <5 %

Fig 12. Probable density distribution of the MX-80 grain assemblages in Fig 11. Total bulk density of the clay after saturation 1.5-1.7 t/m^3

Fig 12 shows that although the grain orientation has some impact on the degree of homogenization of Na montmorillonite clay, its general microstructure features are mainly determined by the initial size distribution of the powder grains. The pictures indicate that for a bulk density of 1.5-1.7 t/m^3, about 5-10 % of an arbitrary cross section represents clay gels with a high content of mobile water (ρ_m = 1.1-1.3 g/cm^3)* and that only about 0.5-2 % intersect very open gels (ρ_m 1.1 g/cm^3). It is reasonable to believe that the last-mentioned microstructural components form pore fillings that are responsible for part of the water conductivity, but since the degree of interconnectivity is higher of the clay gel of "intermediate permeability", i.e. 1.1-1.3 g/cm^3 the latter is probably a determinant of the percolation of water.

The micrograph in Fig 13 illustrates that a Na montmorillonite gel with a bulk density of about 1.3 t/m^3 forms a relatively regular, honeycomb-like system of small aggregates with an average size of interaggregate pores of about 1 µm and an average size of all pores of 0.1-0.5 µm. At lower gel densities the voids are naturally larger.

2.3.3.2 Dense Na montmorillonite clay

The conclusion from the preceding discussion of soft "artificial" Na montmorillonite clay that the initial arrangement of the powder grains determines the geometry of potential flow paths, applies also in the case of compacted powders. This can be imagined by considering the theoretical case of strong isotropic compaction of the particle assemblage termed "a" in Fig 11. As shown in Fig 14 intense compaction is expected to yield a dense layering of distorted grains with much elastic energy stored in the system. Irrespective of the compaction pressure there will be a certain frequency of open voids with a maximum size of 50-100 µm, which may be compressed to 10-20 µm after complete saturation and swelling of the grains. These voids are expected to be invaded by montmorillonite flakes which emerge from

---

* In order to distinguish between the different microstructural components we express the density of the pore-filling gels in g/cm^3, while the bulk density of the total mass is expressed in t/m^3, keeping in mind that 1 g/cm^3=1 t/m^3.

the expanded, dense grains and form a gel with a bulk density of "intermediate" permeability as in the previously discussed softer clays. While this microstructural component may represent 5-10 % of an arbitrary cross section in softer clays, it is assumed to form only 0.5-1 % in heavily compacted, saturated Na montmorillonite clay.

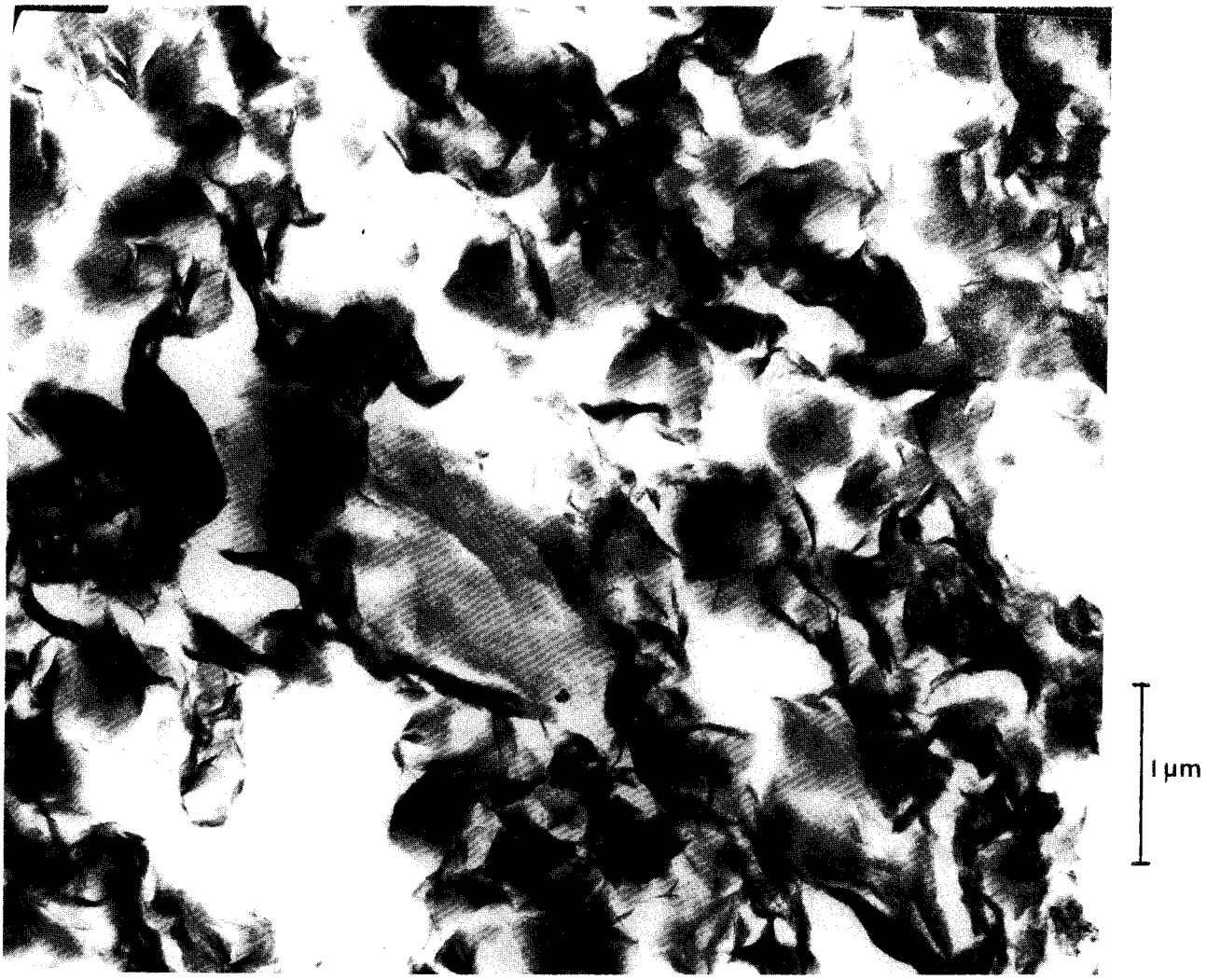

Fig 13. Electron micrograph of ultrathin section of Na montmorillonite with a bulk density of about 1.3 t/m^3

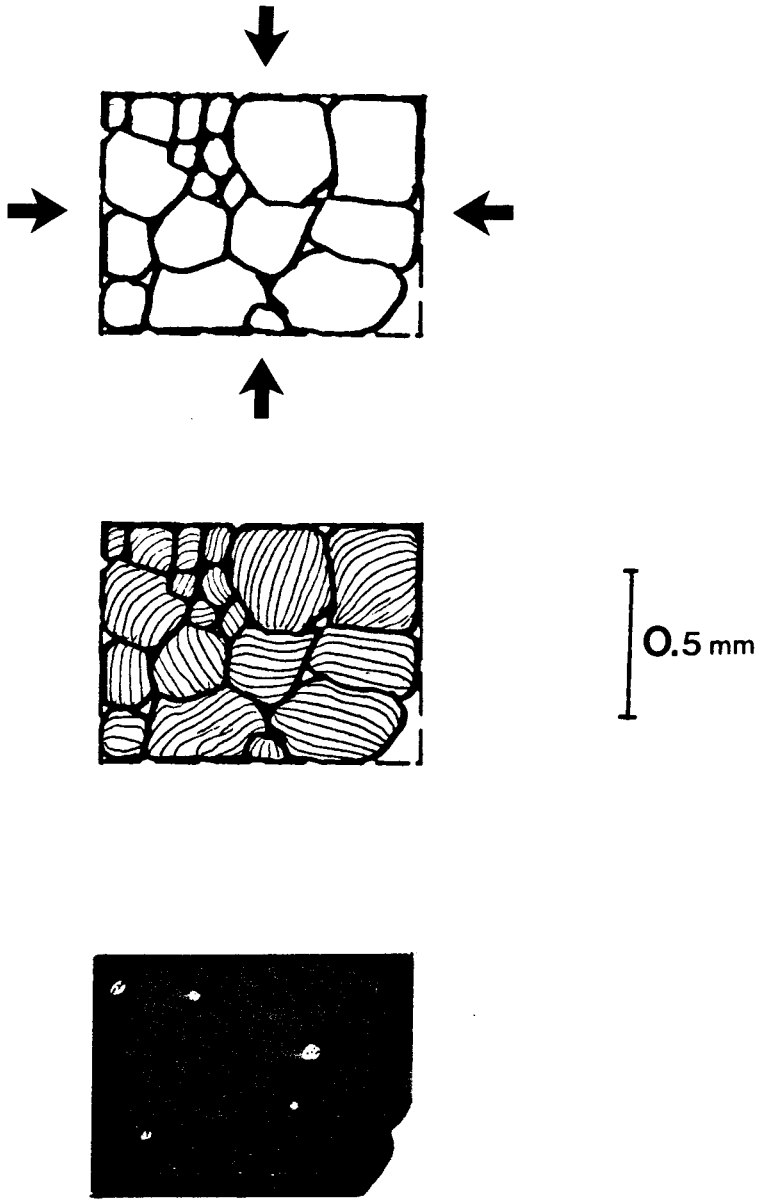

Fig 14. Probable density distribution of compacted MX-80 grain assemblage shown in Fig 12. Total bulk density 2.1 t/m³ after saturation

3 OUTLINE OF MICROSTRUCTURE MODEL OF "ARTIFICIAL" SMECTITE CLAY

3.1 General aspects

A key feature of the microstructural model of artificial Na montmorillonite clay that will be outlined in this report is that its bulk hydraulic conductivity is governed by the clay gel that is formed in the voids between expanded powder grains. At bulk densities higher than 1.5-1.7 t/m^3 there are probably no unfilled voids which are larger than about 1 μm and this means that the gross hydraulic conductivity of such clays is determined by the fraction of an arbitry cross section that is occupied by soft gels.

Assuming that this fraction is 5-10 % for clays with a bulk density of 1.5-1.7 t/m^3, the average hydraulic conductivity would thus be roughly 5-10 % of that of the void-filling gels if there is no variation in interconnectivity. If the gels are assumed to have an average density of 1.3 g/cm^3 and a hydraulic conductivity of 10^{-11} m/s, clays with a bulk density of 1.5-1.7 t/m^3 would be expected to have an average hydraulic conductivity of $5 \cdot 10^{-13}$ to 10^{-12} m/s which is in reasonable agreement with experience. For highly compacted Na montmorillonite the value would be $5 \cdot 10^{-14}$ to 10^{-13} m/s, which is also on the right order of magnitude, indicating that the model of soft gels filling the voids between grains in moderately and densely compacted "artificial" Na montmorillonite clays is reasonable with respect to the permeability. The absence of such "self-healing" void fillings in illitic clay with a bulk density of 1.5-1.7 t/m^3 is aptly demonstrated by the diagram in Fig 15, which shows a plotting of the hydraulic conductivity of such clays related to P/T. We see that there is a general relationship between P/T and the hydraulic conductivity, and that the P/T-range is similar to that of Na montmorillonite clays of the same density. The gross hydraulic conductivity of the latter is, however, only about 1 % of that of the illitic clays which is explained by the earlier mentioned fact that wide, open voids forming continuous flow passages give the major contribution to the P/T value of illite clays. While such clays are characterized by

a complex microstructure with a very wide range of void sizes, "artificial" montmorillonite clays formed from bentonite powders appear to have a more regular void pattern.

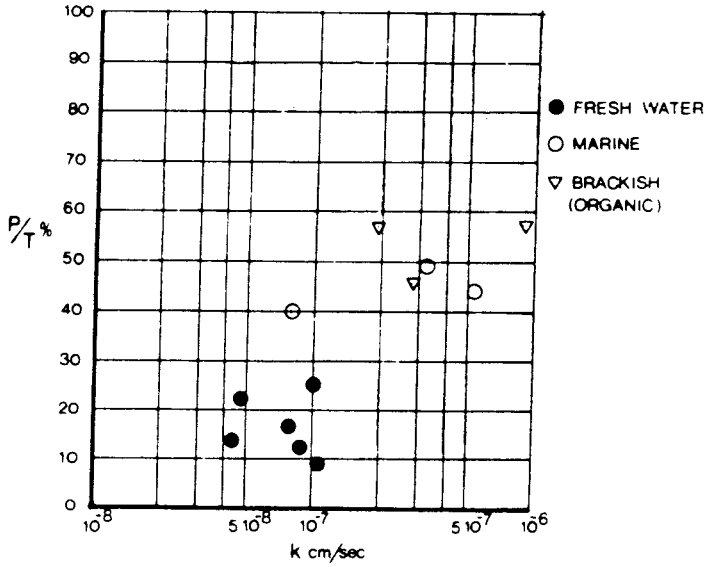

Fig 15. P/T versus hydraulic conductivity k of illitic clays with a bulk density of 1.5-1.7 t/m^3 (8)

3.2 Main features of the model

3.2.1 "Effective" porosity, "external" pores

Referring to the text in the preceding chapters we assume here that air-dry Na montmorillonite in the form of commercial bentonite powder grains consists of large stacks of flakes with one interlamellar water molecule layer. Taking the specific density of the crystal lattice as 2.7 g/cm^3 and the density of the water as 1.0 g/cm^3*, the density of the grains is 2.31 g/cm^3 and the "effective" porosity n, referring to "external" space between the grains, as given in Table 4 for three arbitrarily chosen bulk densities.

---

* The actual density of interlamellar water may be lower than unity, but taking the density of dehydrated montmorillonite as 2.7 g/cm^3 the possible error is insignificant

Table 4. Density and effective porosity (n) of air-dry, smectite-rich powder

Type	Bulk density of air-dry powder t/m^3	Dry density t/m^3	Density at compl saturation t/m^3	n
A	2.0	1.80	2.13	0.13
B	1.5	1.35	1.85	0.35
C	1.0	0.90	1.57	0.57

Water uptake and expansion of the grains to hold 2 or 3 interlamellar hydrates yields the theoretical effective porosity given in Table 5. For the highest initial bulk density (Type A) complete uptake to 2 and 3 hydrates is not geometrically possible. A reasonable assumption made here is that 2/3 of the grains expand to host 2 complete hydrates and that no aggregate takes up 3 hydrates.

Table 5. Effective porosity n after expansion of clay types A, B, C under constant volume conditions

	n	
Type	2 hydrates	3 hydrates
A	0.015*	-
B	0.20	0.05*
C	0.47	0.37*

* Matured state. The values used for conductivity calculations

3.2.2 Size distribution of external pores

The external pore volume that remains after the expansion of the grains will not be free from mineral particles. Soft clay gels, emanating from the grains will be formed in the pore space and they will determine the hydraulic conductivity of the bulk clay. The density of these gels is assumed to depend on the size of the external pores, the size distribution of which is assumed to be log normal. In order to reflect the pore size ranges observed for the three

types of clay, means and standard deviations are set to match the following conditions:

I The minimum pore diameter for the three types of clay is 0.1 μm

II For clays A, B, C the maximum pore diameters are 5 μm, 20 μm and 50 μm respectively.

It is further assumed that 95 % of the total pore space falls in the diameter intervals postulated above. The log normal distribution will then, by definition, predict a small portion (2.5 %) of the total external pore space to consist of pores with diameters larger than the maximum value. These pores are treated as maximum diameter pores when computing the hydraulic conductivity, the distribution functions being adjusted accordingly (Fig 16).

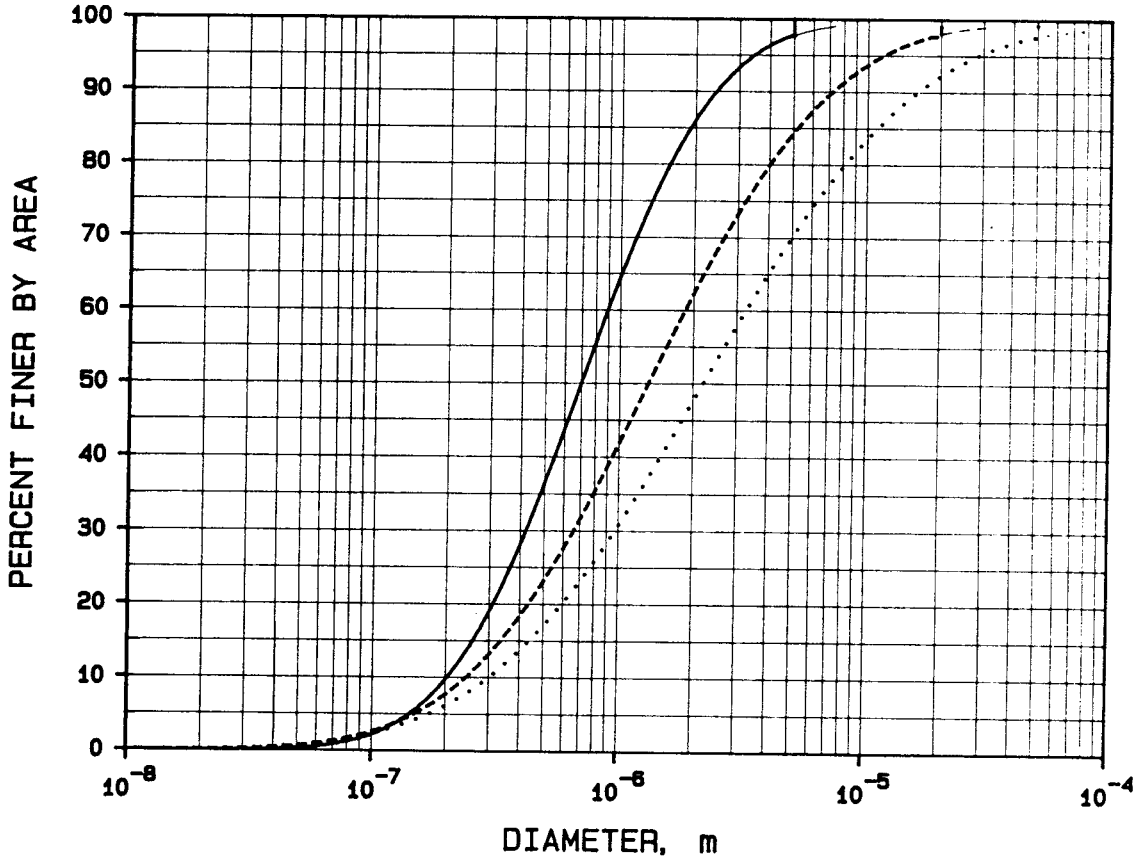

Fig 16. Pore size distribution of clays A, B and C. The fine-pen tails at the upper part of the curves indicate the original log normal distribution functions used for determination of means and standard deviations. Clay A is marked by a full line, B by a broken line and C with a dotted one

Another 2.5 % portion will correspondingly fall outside the lower diameter limit but, having no influence on the conductivity, it does not need to be further considered.

The mean size and standard deviation of the external pores of the three clay types are shown in Table 6, while the fraction of a cross section that is occupied by intersected pores is given by Fig 17. From this figure one finds for example that for Clay A the fraction of intersected pores sized 0.3-1 µm ($3 \cdot 10^{-7}$-10^{-6} m) is approximately $0.65 \cdot 10^{6} \times 0.7\ 10^{-6}$ (mean value for the interval)x(interval length). This yields 0.45, i.e. 45 %. The corresponding fraction for Clay C is only about 20 %. Naturally, this kind of derivation can made more easily by use of the previous diagram.

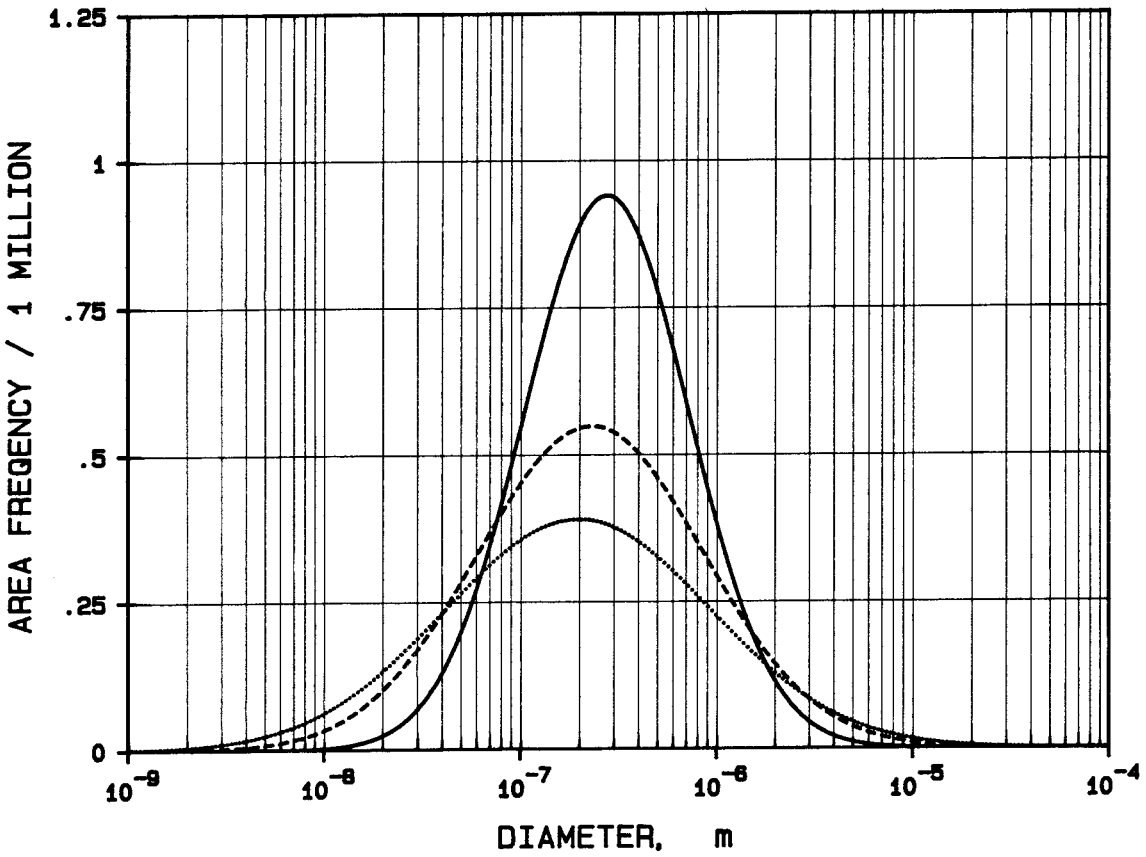

Fig 17. Distribution of the ratio of the pore cross section area and the total cross section area. Clay A is marked by a full line, B by a broken line and C by a dotted one

Table 6. Mean size and standard deviation of external pores

Clay type	Mean value µm	Standard deviation, powers of ten
A	0.70	0.42
B	1.32	0.58
C	2.20	0.68

The actual size range of external pores in matured Na bentonite clay as interpreted from electron micrographs corresponds well with that in Table 6. Thus, microstructural analyses based on scanning microscopy of clays of this sort with a bulk density in the range of that of Clays A and B, indicate an average equivalent diameter of deep-penetrating voids of about 1.2 µm. This is illustrated by the micrographs in Fig 18, which demonstrates that the large majority of the voids are smaller than 1 µm but that there are also a few wider voids like the encircled ones. The lack of gel filling in these voids is only apparent since the freeze-drying caused collapse of the soft gel, which was then lost by the tape peeling that is part of the preparation.

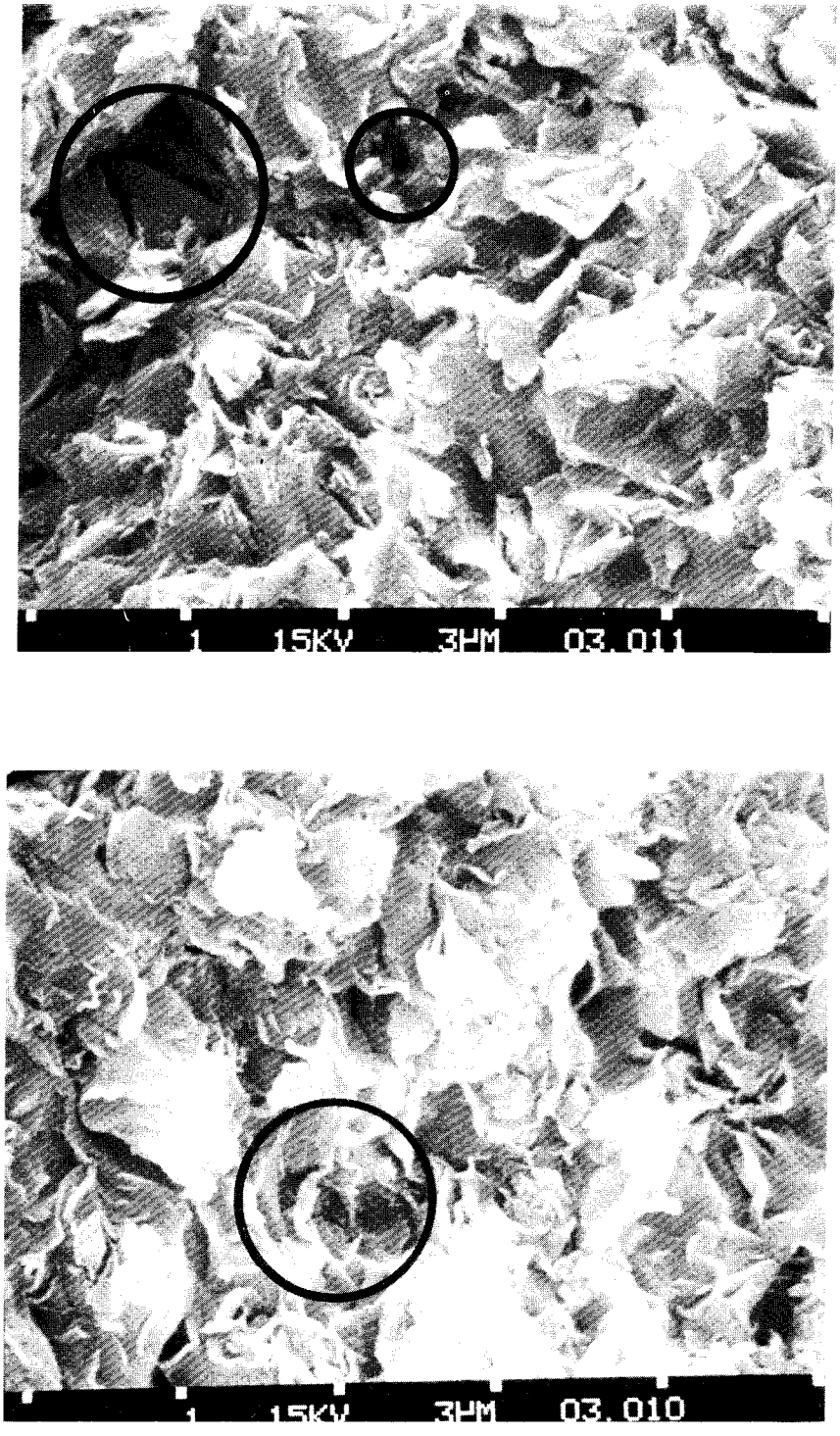

Fig 18. Typical scanning micrographs of matured commercial Na bentonite (MX-80) with a bulk density of 1.9 t/m^3. Probable "external" pores encircled

3.2.3 Density of gels filling external pores

In order to estimate the hydraulic conductivity of the gels in the external pores we first need to calculate their density. At present there is no experimental basis for selecting reliable values but the right order of magnitude can be safely estimated, our choice being that in Table 7.

Table 7. Average clay gel densities in external pores of different size

Pore size interval, μm	Gel density, g/cm³
1 - 5	1.3
5 - 20	1.2
20 - 50	1.1

As to the involved physics it is concluded from various studies (6) that fragments of dense grains become separated and undergo further partial disintegration when they are allowed to expand in open voids, thereby forming the soft gels that we are concerned with here. This process yields the microstructural pattern that is schematically shown in Fig 19. Since the gels emanate from the grains, the size and volume of the latter decrease slightly in the course of the gel formation by which the external porosity is increased. In practice, therefore, the boundaries between the rather massive expanded grains and the soft gels in external pores is of course not as distinct as in this schematic drawing.

In Fig 20 schematic diagrams are shown of the relative amounts of microstructural unity in the three clay types. An important feature of the model, and a prerequisite of its validity, can be implicitely derived from Fig 19, and that is the interconnectivity of the flow passages formed by the gel-filled external pores. Naturally, they do not form straight "capillaries" but winding paths of the sort that can be imagined by applying probabilistic reasonings (10).

The voids of the gel infillings is controlled by the density and the porewater chemistry. Assuming the particles to be arranged in a regular card-house manner, the void size is about 0.05 μm for a gel density of 1.3 g/cm^3 at water saturation, while the corresponding figures are 0.09 and 0.2 μm for the densities 1.2 and 1.1 g/cm^3, respectively. In practice we expect the average void size for fresh-water conditions to be 0.1-0.5 μm depending on the gel density, while brackish water of the Forsmark type is assumed to produce an average void size of 0.2-1 μm for the given gel concentration range. The corresponding build-up of the gels is illustrated by Fig 21, which is meant to illustrate the characteristic microstructural feature of coupled aggregates. They act as rather strong units which move as such under influence of low and moderate shear stresses, and which get torn-off in the course of erosion.

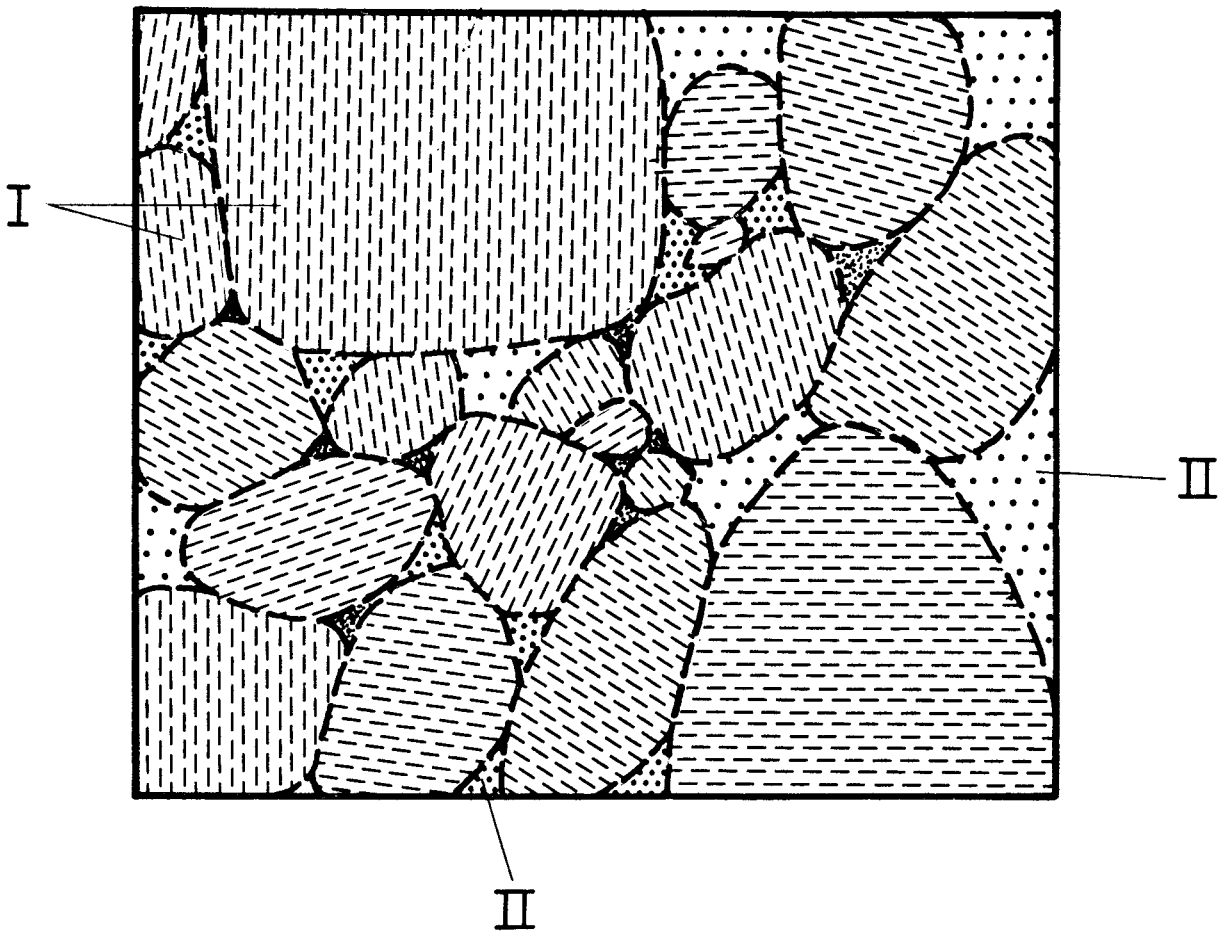

Fig 19. Generalized microstructural pattern of Na montmorillonite clay gel formed from powder grains. I is expanded grain (1-3 interlamellar hydrates), II external pores with gels of different densities

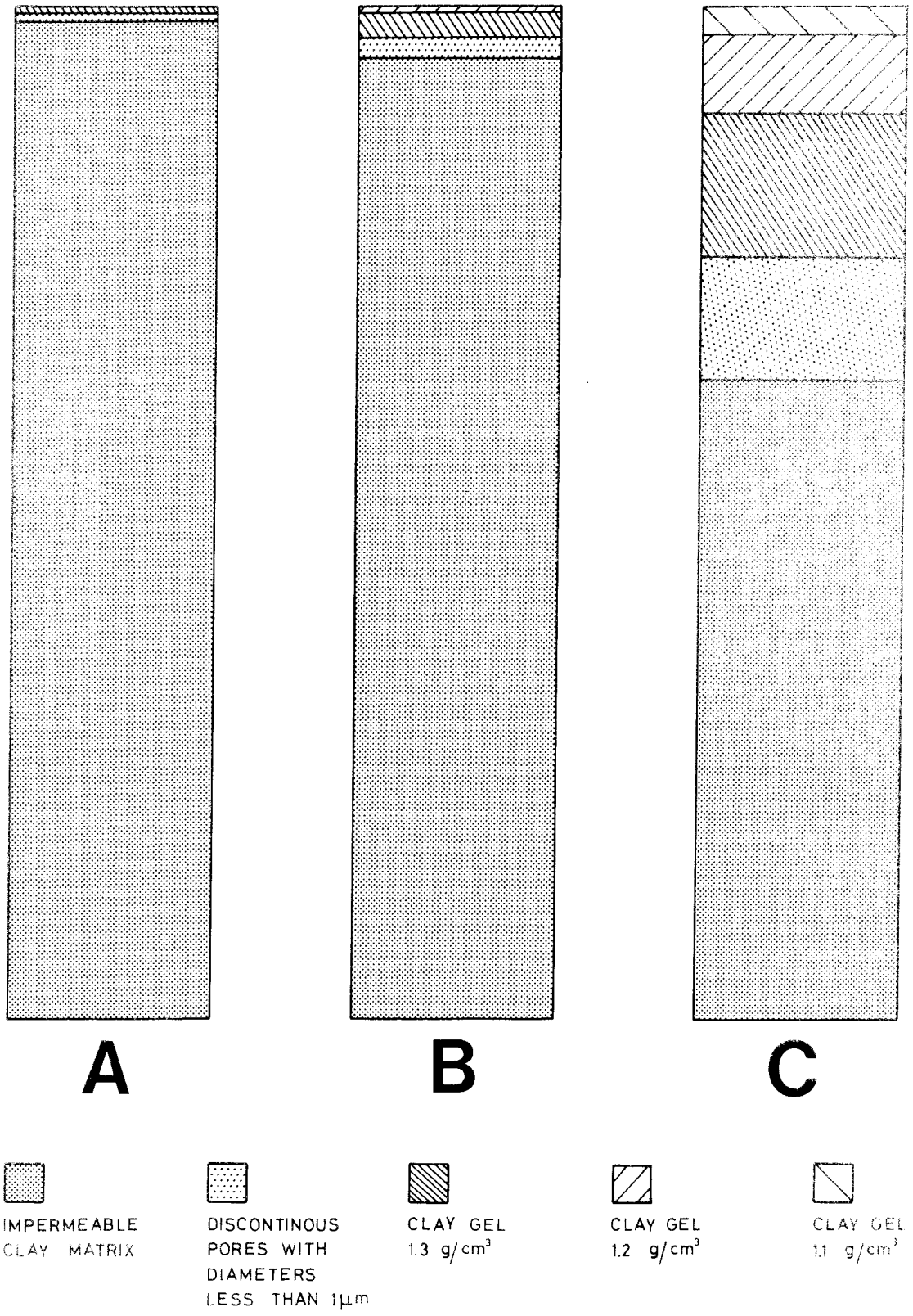

Fig 20. Relative amounts of microstructural units in the three clays A (ρ_d=1.8 t/m³), B (ρ_d=1.35 t/m³) and C (ρ_d = 0.9 t/m³)

Fig 21. The microstructure of gels formed in external pores. Upper: generalized regular pattern of soft aggregates. Lower: Scanning micrograph of freeze-dried specimen with a density of about 1.3 g/cm^3

3.2.4 Hydraulic conductivity of gels filling external pores

A characteristic property of our model is that the gel filling of external pores has a density that depends on their size, which yields a varying hydraulic conductivity over a cross section. Turning back to the diagram in Fig 1 we have a basis for ascribing representative

hydraulic conductivities to the three gel densities specified in Table 8. A distinction is made between the case of practically electrolyte-free porewater, i.e. distilled water, and strongly brackish water with a salinity of about 1/3 of that of the oceans ("Forsmark").

Table 8. Assumed hydraulic density of the clay gels

Gel density g/cm^3	Hydraulic conductivity, m/s	
	Distilled	Forsmark
1.3	10^{-11}	10^{-10}
1.2	10^{-10}	10^{-9}
1.1	10^{-9}	10^{-8}

3.2.5 Hydraulic conductivity of clay in bulk

With the previously defined assumptions we get the distribution of impermeable and permeable fractions of a cross section that is given in Table 9. The resulting average hydraulic conductivity of the three clay types are also given (k_1) as well as representative values of the hydraulic conductivity of laboratory-tested commercial Na bentonites (k_2).

We conclude from Table 9 that the model yields values which are in fair agreement with experimental data. The diagram in Fig 22 illustrates the graphical appearance of the relationship between the average hydraulic conductivity and the dry density of clay in bulk.

Table 9. Distribution of permeable zones and average hydraulic conductivity of clay in bulk at room temperature. k_1 represents the model while the k_2 illustrates typical experimental data

Clay type	Pore water type	Disc pores with diam smaller than 1 µm	Gel fillings with $k=10^{-11}$ m/s	$k=10^{-10}$ m/s	$k=10^{-9}$ m/s	$k=10^{-8}$ m/s	k_1 m/s	k_2 m/s
A	Dist w	64 %	36 %	-	-	-	$5\cdot10^{-14}$	$2\cdot10^{-14} - 10^{-13}$
B	" "	42 %	43 %	15 %	-	-	10^{-12}	$10^{-13} - 10^{-12}$
C	" "	31 %	40 %	22 %	7	-	$4\cdot10^{-11}$	$5\cdot10^{-11} - 10^{-13}$
A	Brackish w	64 %	-	36 %	-	-	$5\cdot10^{-13}$	$10^{-13} - 10^{-12}$
B	" "	42 %	-	43 %	15 %	-	10^{-11}	$5\cdot10^{-12} - 10^{-11}$
C	" "	31 %	-	40 %	22 %	7 %	$4\cdot10^{-10}$	$10^{-10} - 2\cdot10^{-10}$

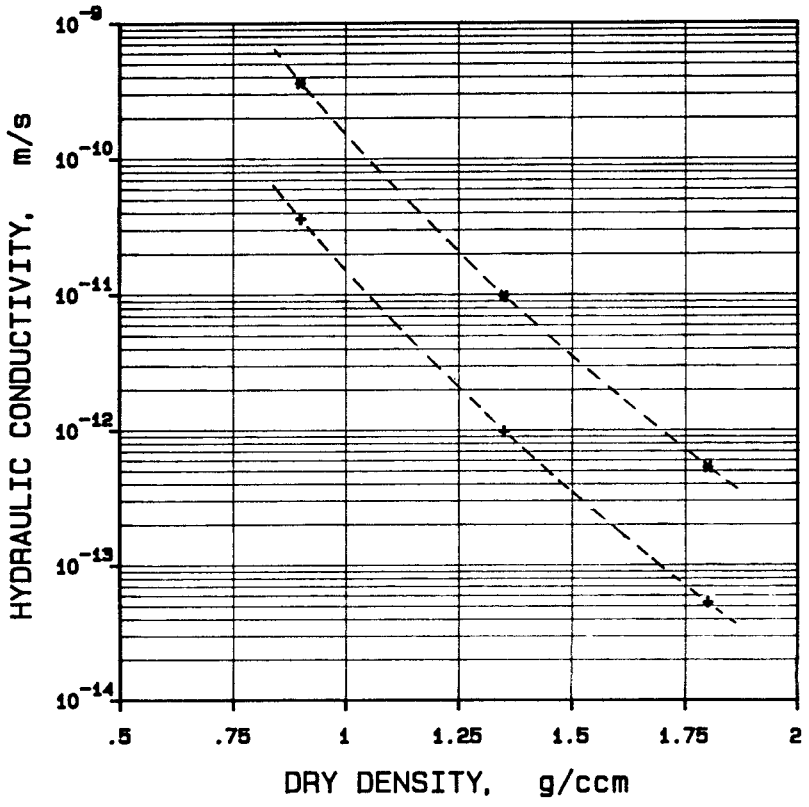

Fig 22. Hydraulic conductivity in bulk versus dry density according to the model. * Forsmark water, + Dist water

3.3 Physical implications of the model

3.3.1 General

Naturally, various microstructural models can be designed so as to yield conductivity data that fit certain laboratory experiments like the ones which we used for back-checking. However, the model must also fit other major soil data and behave according to what is observed in laboratory tests of various kinds. Thus, the relationship between density and swelling pressure and gas conductivity must be at least qualitatively in agreement with what is recorded in the laboratory. Finally, the cation and anion diffusivities must also be in reasonable agreement with the major properties that are familiar from various literature references. We will consider these points and finally draw conclusions as to the water percolation processes in smectite clays with special respect to some major physical and chemical effects.

3.3.2 Swelling pressure

The swelling pressure can be estimated by considering the schematic microstructural arrangement in Fig 19 and the block diagram in Fig 20, which yields the fraction of a cross section that is occupied by aggregates, i.e. the units which are major contributors to the swelling pressure in bulk. Thus, disregarding the gels in the external pores, which can be assumed to give an insignificant contribution, the swelling pressure in bulk can be estimated by use of Eq. (4):

$$p_s = \alpha(\Sigma p_i A_i)/A \qquad (4)$$

where p_s = swelling pressure in bulk
p_i = "true" swelling pressure of aggregates (stacks) with internal water only
α = aggregate orientation factor
A = total area of a unit cross section
A_i = contact area of aggregates in the unit cross section

Assuming that one third of the aggregates are oriented with the crystallographic c-axis in the direction in which the swelling pres-

sure is considered, we get α=1/3. p_i depends on the number of interlamellar hydrate layers in a manner that is controlled by the kind and amount of interlamellar cations. Applying Yong & Warkentin's theory (11) we would expect the true swelling pressure to be related to the number of hydrates as given by Table 10, and taking α=1/3 and calculating A_i/A from the ratio of "the impermeable clay matrix" area and the total area of the respective columns in Fig 20, we arrive at the average bulk swelling pressures given in Table 11, which also comprises representative laboratory test results.

Table 10. Theoretical, "true" swelling pressure of sodium montmorillonite (12)

Number of interlamellar hydrates	p_i MPa
1	17
2	8
3	5

Table 11. Swelling pressure of clay in bulk. p_{s1} refers to the model, while p_{s2} represents characteristic laboratory test values

Clay type	p_i MPa	A_i/A	p_{s1} MPa	p_{s2} MPa
A*	12	0.99	3.8	10 - 15
B	5	0.95	1.6	0.5-1.5
C	5	0.64	1.1	<0.2

* Assuming 2/3 of the aggregates to host 2 interlamellar hydrate layers and the rest 1 hydrate layer

We conclude from Table 11 that the model yields swelling pressure values that are in reasonable agreement with recorded ones for a bulk dry density of 1.35 t/m^3 (Clay B), while for low densities (Clay C) the model yields values that are significantly higher than typical

recorded values. This may be explained by microstructural effects. Thus, considering the frequent defects and deviation from a perfect stacking of the mineral flakes, the expansion of the grains in Clay C to hold 3 interlamellar hydrate layers is probably associated with a considerable loss in continuity and stress transfer within the stacks. The underestimation of the swelling pressure of the dense Clay A is due to incorrect assumptions that form the basis of the Yong/ Warkentin theory for single interlamellar hydrate layers of sodium montmorillonite as pointed out by various investigators (13). Thus, strong mineral/water interaction through hydrogen and van der Waals bonds yields a much higher swelling pressure than the osmotic pressure that is taken as the basis of the Yong and Warkentin model.

3.3.3 Gas conductivity

Several investigations have demonstrated that gas penetrates smectite clays in gaseous form when the pressure is sufficiently high (14, 15). This migration takes place through a few wide passages as observed in gas conductivity tests. It has been demonstrated that the critical pressure is very much dependent on the bulk density of the clay (cf. Table 12) and that this pressure can be predicted by considering the pore system to be equivalent with quartz capillaries. This yields the values in Table 13 and from Tables 12 and 13 we conclude that our reference clay types should have a maximum pore diameter of about 0.1 μm for Clay A, 2 μm for Clay B, and 20 μm for Clay C in order to fit the capillary analogy. For Clay A this figure agrees rather well with the actual void size (0.1-0.2 μm) of the gel in the external pores, while for Clay B there is less good agreement with the gel void size (0.2-0.5 μm). For Clay C the analogy even requires a 20 times larger gel void size than the actual one in order to yield a representative critical pressure, the discrepancy being explained by the low mechanical strength of the gel. Thus, it is logical to believe that when gas penetrates the relatively large external pores filled with 1.1 g/cm^3 clay gel, this gel is displaced and opens the largest external pores to a width that may approach the original one, i.e. 20-50 μm. This effect can be assumed to be initiated also at bulk densities represented by Clay B.

Even for higher dry densities than that of Clay B the penetration of gas requires some displacement of the clay gel, and since this affects also the system of densely layered stacks which are strongly pressed together, it is logical to believe that the critical gas pressure is on the same order of magnitude as the swelling pressure for clays of high density.

Table 12. Compilation of experimental data on the critical gas pressure (p_g) of commercial Na bentonites (15)

ρ_d, t/m³	p_g, kPa
0.87	15
0.95	60
1.00	60
1.08	160
1.40	1600
1.46	2400
1.62	5000
1.71	5000
1.75	11000
1.78	19000
1.79	21000

Table 13. Critical pressure (p_g) in quartz capillaries (15)

D, μm	p_g, kPa
200	1.5
150	3
40	7
20	14
10	30
4	70
2	140
1	300
0.1	3000
0.01	30000

3.3.4 Diffusion

The model implies that regularly ordered stacks holding only internal water and exchangeable cations in interlamellar positions do not allow for anion migration, while cations may or may not diffuse through the aggregates depending of their size and charge. Since the external pores, filled with clay gels of varying density, offer the only pathways for anions the diffusion capacity should be roughly proportional to the "effective" porosity (Table 5), which, after complete maturation, is 0.015 for Clay A and 0.05 and 0.37 for Clays B and C, respectively. Assuming that cation diffusion takes place through the entire water-filled space represented by the total porosities 0.34, 0.50, and 0.66 for Clays A, B, and C, it is concluded that the anion diffusion capacity is about 5 % of that of cations for Clay A, while the corresponding figure is roughly 10 % for Clay B and 55 % for Clay C. Data from diffusion experiments with clays of a bulk density similar to that of Clay A, i.e. about 2.1 t/m^3, confirm that this ratio is actually only a few percent (16).

The exclusion of anions from regularly organized stacks of flakes expanded to hold up to 3 hydrate layers in interlamellar positions does not imply that anion diffusion takes place exclusively in the gel-filled external pores. Thus, considering the frequent structural defects of bentonite grains in the form of openings that are wide enough to permit development of electrical double-layers and formation of mobile water with freely moving ions (cf. Fig 3), it is clear that migration of ions takes place into many "dead end" pores in large stacks like those termed I in Fig 19. In agreement with the hypothesis of Torstenfelt and Allard (17) this would lead to two apparently different anion diffusion mechanisms with a deviation from the theoretical concentration profile representing simple "pore diffusion". The processes combine to yield an excess concentration at small distances from the ion source in short term laboratory experiments as illustrated by the diagram in Fig 23. Cations which are small enough to pass through interlamellar space, like Na and Li, are not expected to exhibit the same diffusion pattern, while certain large cations which are excluded from interlamellar positions for geometrical and charge reasons are assumed to behave in a similar way as anions.

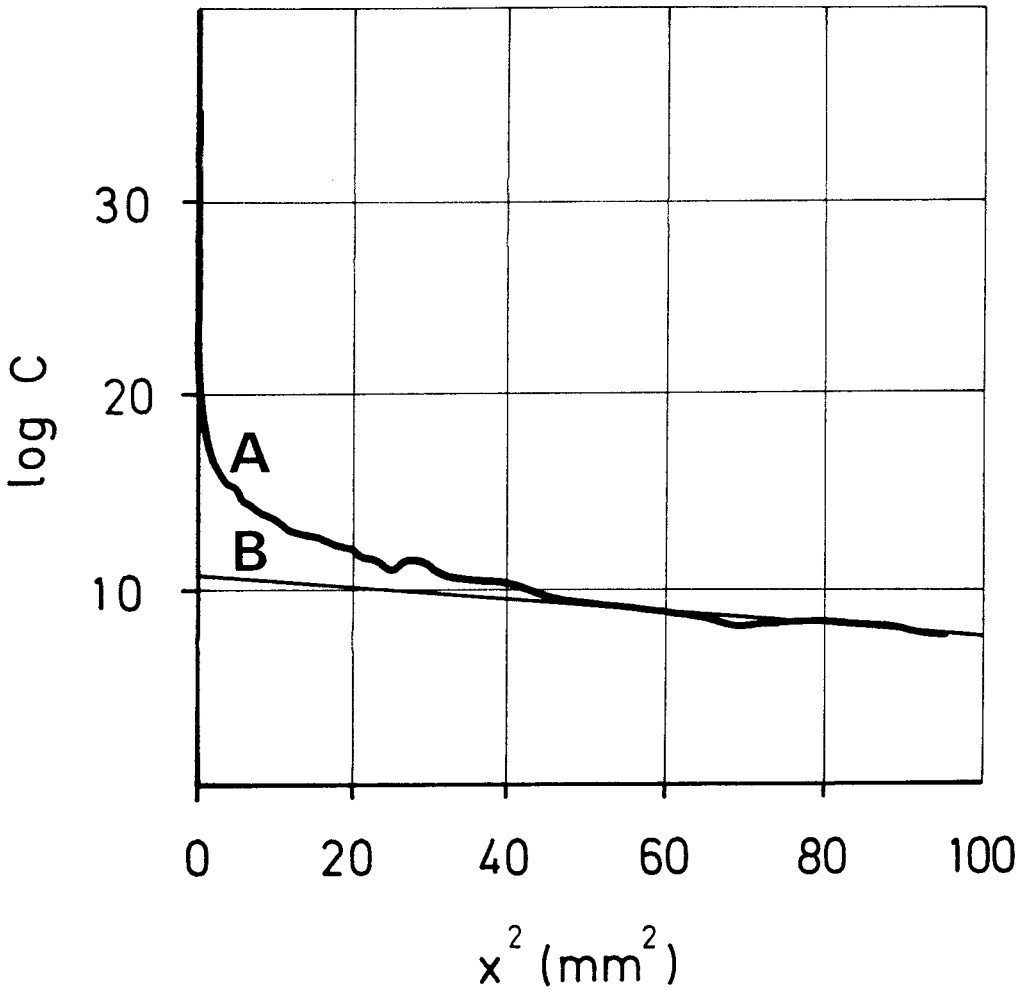

Fig 23. Diffusion of iodine in Na bentonite (ρ_m = 2.0 t/m³), the profile determined 157 days after start (17). C is concentration, x distance from ion source

3.3.5 Uniformity of water percolation

The flow model described in this report implies a large variation in flow rate and capacity of the permeable intergranular passages. This means that major parts of the clay matrix will not be permeated at all while certain very narrow zones will be percolated at a very high rate. A positive effect of this variation is that the migration of certain dissolved substances that can attack the clay minerals or canisters embedded in the clay mass, will be very much delayed and the solution may not even react at all with large parts of the permeated mass. This effect is illustrated by a test in which a strong NaOH base was percolated through a highly compacted Na bentonite sample. Although the amount of solution that was forced through the sample corresponded to 16 times the total pore volume during the

1 year long test, no measurable effect on the montmorillonite minerals could be detected (18).

The variation in flow rate over a cross section of Na smectite clay according to our model is amply illustrated by the three clay types A, B and C as depicted in Figs 24-26. They show square-shaped cross sections with a side length of 250 μm from which we see that Clay A, with a dry density of 1.8 t/m^3, has a fairly homogeneous structure with an apparently uniform percolation rate of the 1-5 μm wide gel-filled pores. We note that the pores are widely separated by large impervious parts of the clay matrix.

Clay B, with a dry density of 1.35 t/m^3, has a certain, small number of 5-20 μm wide, gel-filled pores which let water through at a rate that is 10 times higher than that of the 1-5 μm pores. As to Clay C, finally, we see that in this soft clay (ρ_d=0.9 t/m^3) there are a few 20-50 μm wide pores filled with a soft clay gel. These pores are responsible for 72 % of the flow and yield flow rates which are 100 times higher than that of the 1-5 μm pores.

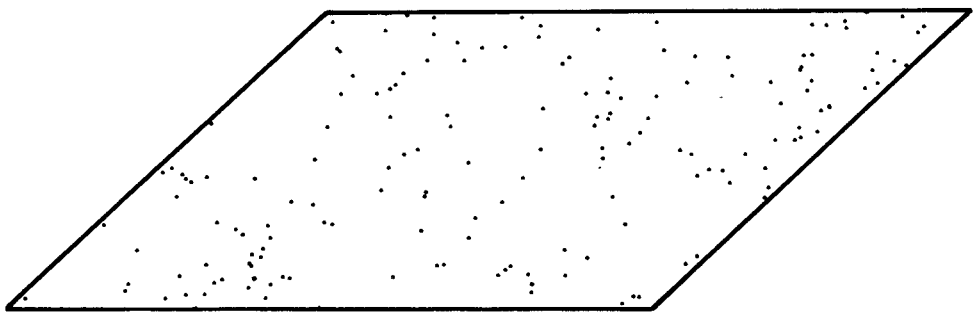

Fig 24. Flow rate distribution in Clay A. Dots represent external gel-filled pores sized 1-5 μm. The total number is 168 over the 250x250 μm cross section area

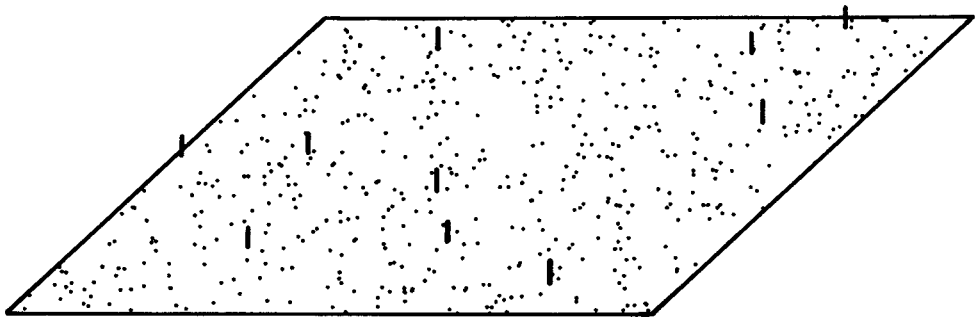

Fig 25. Flow rate distribution in Clay B. Dots represent 1-5 μm pores and short bars 5-20 μm gel-filled external pores. The numbers are 547 and 10, respectively, per 250x250 μm cross section area

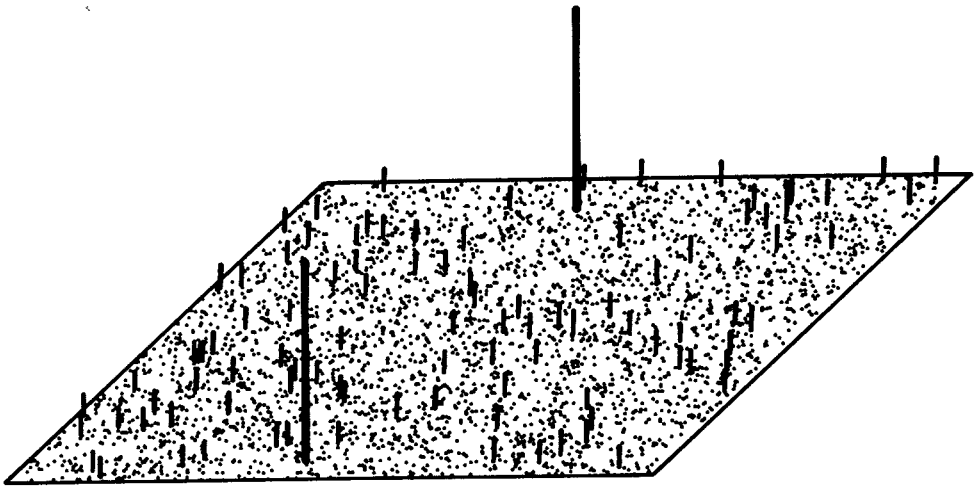

Fig 26. Flow rate distribution in Clay C. Dots represent 1-5 μm pores, short bars 5-20 μm pores, and the long bars 20-50 μm gel-filled external pores. The numbers are 3400, 100, and 2, respectively, per 250x250 μm cross section area

A negative effect of the variation in flow rate is that the locally occurring rapid percolation may affect the mechanical stability of soft gels in the external pores. Thus, the average flow rate at a hydraulic gradient of 50 is on the order of 10^{-6} m/s in the widest gel-filled pores of Clay C, and this is sufficient to distort the softest gels i.e. those with a bulk density of about 1.1 g/cm^3. True erosion in the form of disintegration and washing out of small clay aggregates over large distances will not take place at this moderate flow rate (19) but the probable slight displacements that the gel undergoes will lead to a time-dependent change in bulk hydraulic conductivity as illustrated by Fig 27. It is clear that gradients on the order of 10^3 to 10^4, which are often applied in laboratory investigations, certainly produce microstructural alterations.

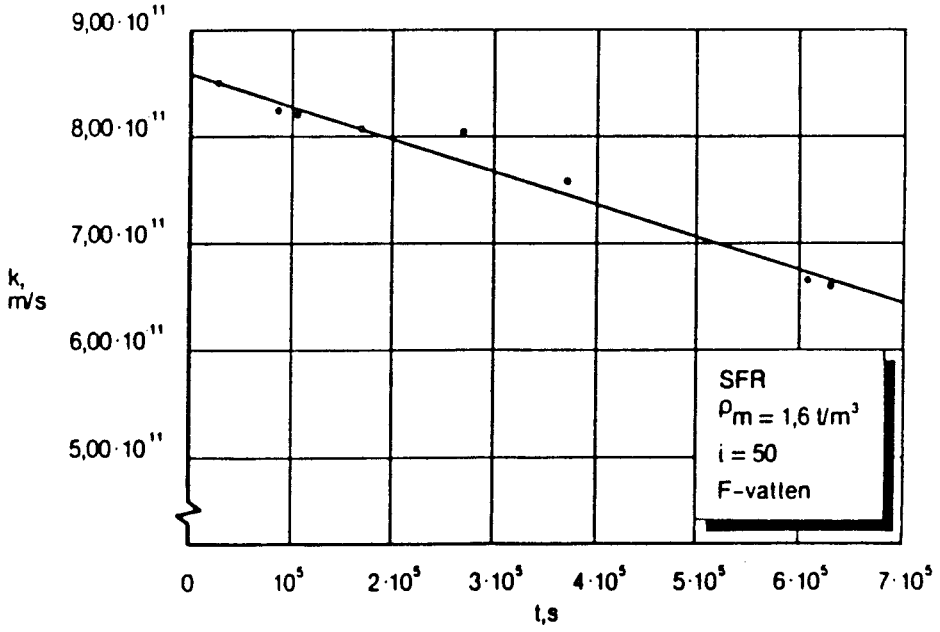

Fig 27. Time-dependent change in hydraulic conductivity of GEKO/QI bentonite with a dry density of 0.95 t/m^3, percolated by Forsmark water at a hydraulic gradient of 50

4 CONCLUSIONS, RECOMMENDATIONS

A general, main conclusion from the study is that the microstructure of "artificial" Na montmorillonite clays formed from bentonite powder grains, controls all the important transport mechanisms. The key feature of the microstructural model is that the dense grains constitute a basic network with continuous "external" pores of varying size. At hydration of the system under confined conditions the grains expand and reduce the porosity, and the remaining voids then become filled by soft clay gels that emanate from the dense grains. The density of the gels is a function of the void size, which means that there is a variation in hydraulic conductivity and mechanical strength of the gel fillings. This type of model would explain a number of the laboratory-derived physical and physico/chemical properties of such "artificial" clays, the major points being:

1 Complete structural homogeneity will never be arrived at. One consequence of this is that there will always be a number of relatively conductive flow passages even at very high bulk densities, meaning that there is no treshold gradient for initiating water flow. At moderate and high bulk densities large parts of the clay matrix are impermeable, however.

2 The empirical finding that the critical gas pressure is very much dependent on the bulk density is explained by the associated variation in mechanical strength of the gel fillings. The small intergranular pores at high bulk densities yield denser and stronger gel fillings than in less dense clays, which results in higher critical gas pressures at high densities.

3 Even at very high densities the bulk hydraulic conductivity is a function of the porewater chemistry. This can only be explained by the feature of "fibrous" continuous passages of soft clay gels which are sensitive to the composition and concentration of cations in the water.

4 The laboratory-derived conclusion that the anion diffusion capacity of dense clays is very much smaller than that of cations, is nicely explained by the dominance of dense grains with small interlamellar spacing and Donnan exclusion of anions.

In order to check the model more thoroughly and to refine it, the following steps should be taken:

* Transmission electron and optical microscopy of matured clay of various density and age to quantify the microstructure

* Percolation experiments with tracers to identify the pathways by use of microscopy and autoradiography

* Diffusion experiments for determination of the anion/cation diffusion capacity ratio of soft clays, as well as for identification of pathways by use of electron microscopy and element analyses

* Compaction experiments with Fuller-type grain distribution of bentonite powder in order to reduce the size of "external" pores and improve the microstructural homogeneity

5 ACKNOWLEDGEMENTS

The authors are greatly indebted to Rolf Odselius, Dep of Pathology, University of Lund, for very valuable assistance in running part of the scanning microscopy.

Thanks are extended to Jeanette Stenelo for the excellent word processing and to Birgitta Hellström for her careful preparing of the drawings.

6 REFERENCES

1 Mesri, G. & Olson, R.E. Mechanisms Controlling the Permeability of Clays. Clays and Clay Minerals, Vol. 19, 1971 (pp. 151-158)

2 Börgesson, L. & Pusch, R. Basic Properties of Bentonite-based Buffer Materials and Their Function in WP-cave Repositories. SGAB Int. Report IRAP 86501, 1986

3 Pusch, R. Clay Microstructure. Document D8:1970. Nat. Swed: Build. Res: Council

4 Delage, P. & Lefebvre, G. Study of the Structure of a Sensitive Champlain Clay and of Its Evolution During Consolidation. Can. Geot. J. Vol. 21, No. 1, 1984

5 Bennett, R.H. & Hulbert, M.H. Clay Microstructure, IHRDC Publ., Boston, 1986

6 Pusch, R. Identification of Na Smectite Hydration by Use of "Humid Cell" High Voltage Microscopy. Applied Clay Science, Elsevier Publ. Co (In press)

7 Pusch, R. & Karnland, O. Aspects of the Physical State of Smectite-adsorbed Water. SKB Technical Report 86-25, 1986

8 Pusch, R. Influence of Salinity and Organic Matter on the Formation of Clay Microstructure. Proc. Int. Symp. on Soil Structure, Gothenburg 1973

9 Pusch, R. Influence of Organic Matter on the Geotechnical Properties of Clays. Document D11:1973, Nat. Swed. Build. Res. Council

10 Pusch, R. Radionuclide Migration by Water Flow and Diffusion through Smectite Barriers. Proc. Workshop on Mathematical Modelling for Radioactive Waste Repositories, ENRESA, Madrid, 1986

11 Yong, R. & Warkentin, B.P. Soil Properties and Behaviour. Elsevier Publ. Co., Amsterdam, 1975 (449 pp)

12 Pusch, R. Engineering Aspects of Clay-weathered Blekinge Gneiss. Geologiska Föreningens i Stockholm Förhandlingar, Vol. 101, Pt. 1, 1979 (pp. 27-31)

13 Pusch, R. Mineral-water Interactions and Their Influence on the Physical Behavior of Highly Compacted Na Bentonite. Can. Geot. J., Vol. 19, No 3, 1982 (pp. 381-387)

14 Pusch, R., Ranhagen, L. & Nilsson, K. Gas Migration through MX-80 Bentonite, Final Report. Technical Report 85-36, NAGRA, 1985

15 Pusch, R. & Hökmark, H. Megapermeameterstudie av Gastransport genom SFR-buffertar. Arbetsrapport SFR (In press)

16 Pusch, R. & Carlsson, T. The Physical State of Pore Water of Na Smectite Used as a Barrier Component. Eng. Geol., Vol. 21, 1985 (pp 257-265)

17 Torstenfelt, B. & Allard, B. Migration of Fission Products and Actinides in Compacted Bentonite. SKB Technical Report 86-14, 1986

18 Pusch, R. Chemical Interaction of Clay Buffer Materials and Concrete. Arbetsrapport SFR 82-01, 1982

19 Pusch, R., Erlström, M. & Börgesson, L. Piping and Erosion Phenomena in Soft Clay Gels. SKB Technical Report (In Press)

List of SKB reports

Annual Reports

1977–78
TR 121
KBS Technical Reports 1 – 120.
Summaries. Stockholm, May 1979.

1979
TR 79–28
The KBS Annual Report 1979.
KBS Technical Reports 79-01 – 79-27.
Summaries. Stockholm, March 1980.

1980
TR 80–26
The KBS Annual Report 1980.
KBS Technical Reports 80-01 – 80-25.
Summaries. Stockholm, March 1981.

1981
TR 81–17
The KBS Annual Report 1981.
KBS Technical Reports 81-01 – 81-16.
Summaries. Stockholm, April 1982.

1982
TR 82–28
The KBS Annual Report 1982.
KBS Technical Reports 82-01 – 82-27.
Summaries. Stockholm, July 1983.

1983
TR 83–77
The KBS Annual Report 1983.
KBS Technical Reports 83-01 – 83-76
Summaries. Stockholm, June 1984.

1984
TR 85–01
Annual Research and Development Report 1984
Including Summaries of Technical Reports Issued during 1984. (Technical Reports 84-01– 84-19)
Stockholm June 1985.

1985
TR 85-20
Annual Research and Development Report 1985
Including Summaries of Technical Reports Issued during 1985. (Technical Reports 85-01-85-19)
Stockholm May 1986.

1986
TR86-31
SKB Annual Report 1986
Including Summaries of Technical Reports Issued during 1986
Stockholm, May 1987

Technical Reports

1987

TR 87-01
Radar measurements performed at the Klipperås study site
Seje Carlsten, Olle Olsson, Stefan Sehlstedt, Leif Stenberg
Swedish Geological Co, Uppsala/Luleå
February 1987

TR 87-02
Fuel rod D07/B15 from Ringhals 2 PWR: Source material for corrosion/leach tests in groundwater
Fuel rod/pellet characterization program part one
Roy Forsyth
Studsvik Energiteknik AB, Nyköping
March 1987

TR 87-03
Calculations on HYDROCOIN level 1 using the GWHRT flow model
Case 1 Transient flow of water from a borehole penetrating a confined aquifer
Case 3 Saturated-unsaturated flow through a layered sequence of sedimentary rocks
Case 4 Transient thermal convection in a saturated medium
Roger Thunvik, Royal Institute of Technology, Stockholm
March 1987

TR 87-04
Calculations on HYDROCOIN level 2, case 1 using the GWHRT flow model
Thermal convection and conduction around a field heat transfer experiment
Roger Thunvik
Royal Institute of Technology, Stockholm
March 1987

TR 87-05
Applications of stochastic models to solute transport in fractured rocks
Lynn W Gelhar
Massachusetts Institute of Technology
January 1987

TR 87-06

Some properties of a channeling model of fracture flow

Y W Tsang, C F Tsang, I Neretnieks
Royal Institute of Technology, Stockholm
December 1986

TR 87-07

Deep groundwater chemistry

Peter Wikberg, Karin Axelsen, Folke Fredlund
Royal Institute of Technology, Stockholm
June 1987

TR 87-08

An approach for evaluating the general and localized corrosion of carbon steel containers for nuclear waste disposal

GP March, KJ Taylor, SM Sharland, PW Tasker
Harwell Laboratory, Oxfordshire
June 1987

TR 87-09

Piping and erosion phenomena in soft clay gels

Roland Pusch, Mikael Erlström,
Lennart Börgesson
Swedish Geological Co, Lund
May 1987